Supporting Information

Proton-conducting coordination polymers formed from bipyridine phosphonate ligands

Prajakta Mohan Ramteke,[†‡] Tomáš Plecháček,[$] Matouš Kloda,[†] Jan Rohlíček,[§] Anna Vykydalová,[†‖] Klára Melánová,[$] Dmytro Bavol,[†] Karel Škoch,[†] Marco Taddei,[⊥] Jan Demel,[†] Jan Hynek,[†*]

† Institute of Inorganic Chemistry of the Czech Academy of Sciences, Husinec-Řež 1001, 25068 Řež, Czech Republic; E-mail: hynek@iic.cas.cz

‡ Department of Inorganic Chemistry, Faculty of Science, Charles University, Hlavova 2030, 128 40 Prague, Czech Republic

$ Center of Materials and Nanotechnologies, Faculty of Chemical Technology, University of Pardubice, Studentská 95, 53210 Pardubice, Czech Republic

§ Institute of Physics of the Czech Academy of Sciences, Na Slovance 1999/2, 18221 Praha, Czech Republic

‖ Polymer Institute, Slovak Academy of Sciences, Dúbravská Cesta 9, 84541, Bratislava, Slovakia

⊥ Department of Chemistry and Industrial Chemistry, INSTM Research Unit, University of Pisa, Via G. Moruzzi 13, Pisa I-56124, Italy

Table of Contents_Toc219829629

Experimental details

Materials:

4,4'-Bipyridine (BLDpharm), triethyl phosphite, ethyl chloroformate, sodium hydrogen carbonate (ACS reagent, anhydrous, all Sigma-Aldrich), acetic acid (99.8% G.R.), hydrogen peroxide (30%, non-stabilized), ethyl acetate, methanol (G.R. ISO reagent), dichloromethane, hydrochloric acid (35%) (all Lach:Ner, Czech Republic), Acetone (VWR Chemicals) were used as purchased. Acetonitrile (VWR chemicals) for synthesis was dried using solvent purifier SP-1 (LC Technology solutions). Standard Schlenk technique was used to synthesize phosphonate esters under Ar atmosphere. Column chromatography was performed on neutral aluminium oxide (Brockmann I, 40-300 μm, 60A). Ultrapure water from Direct-Q 3 UV water purification system was used for all the aqueous methodologies.

Synthesis of the organic linkers

Preparation of 4,4′-bipyridine-N,N′-dioxide (1).

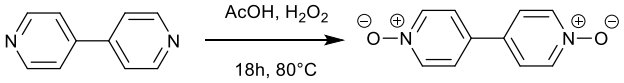

A mixture of 4,4'-bipyridine (5.0 g, 0.032 mol), 35% hydrogen peroxide (7.0 mL) and acetic acid (36 mL) was heated overnight at 80 °C. The resulting solution was evaporated to dryness in vacuum and recrystallized from water (approx. 50 mL) by addition of an excess of acetone (approx. 200 mL). The suspension was kept in a refrigerator for 3–4 h, the precipitate was collected by vacuum filtration and air dried. Product was obtained as white crystalline solid.

Yield: 5.93 g (98 %)

^{1}H NMR (D_2O): 8.24 (m, 1H), 7.79 (m, 1H)

^{13}C{^{1}H} NMR (D_2O): 139.5, 138.0, 124.8

Characterization data correspond to those previously reported in literature (J. Jia, A.J. Blake, N.R. Champness, P. Hubberstey, C. Wilson, M. Schröder, *Inorg. Chem*. **2008**, 47, 8652)

HRMS (APCI) $[M+H]^+$: m/Z calculated for $C_{10}N_2O_2H_9^+$: 189.0664; found: 189.0654

Preparation of tetraethyl 4,4′-bipyridine-2,2′-bisphosphonate (2).

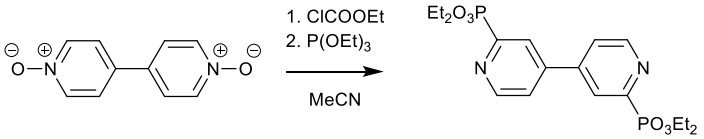

A Schlenk tube was charged with 5.93 g of **1** (0.032 mol), evacuated and flushed three times with argon, and the content was dissolved in acetonitrile (approx. 500 mL). The solution was stirred and six equivalent of ethyl chloroformate (0.19 mol) was added dropwise to the solution. The reaction mixture was stirred for 60 min at room temperature, thereafter, six equivalent of triethyl phosphite (0.19 mol) was added dropwise and the solution was stirred for another 16 h, at RT. After that, the reaction was neutralised and quenched by the addition of saturated $NaHCO_3$ solution. The product was collected by extraction of the water solution with ethyl acetate. The combined organic fraction was dried over a large amount of Na_2SO_4, evaporated to dryness, and further purified by a column chromatography on neutral aluminium oxide. First, pure dichloromethane was used to wash out the impurities and thereafter the product was eluted by a 9:1 to 8:2 dichloromethane/methanol mixture and obtained as off-white solid.

Yield: 8.5 g (63%)

^{1}H NMR ($CDCl_3$): 8.94 (m, 1H, 6-*CH*), 8.25 (m, 1H, 3-*CH*), 7.70 (m, 1H, 5-*CH*), 4.28 (m, 4H, PO*CH*$_2$CH$_3$), 1.38 (t, $^3J_{HH}$ = 7.1 Hz, 6H, POCH$_2$*CH*$_3$)

^{13}C{^{1}H} NMR ($CDCl_3$): 153.4 (d, $^1J_{PC}$ = 226.8 Hz, 2-C), 151.5 (d, $^3J_{PC}$ = 23.3 Hz, 6-CH), 150.0 (d, $^3J_{PC}$ = 12.7 Hz, 4-C), 125.8 (d, $^2J_{PC}$ = 26.1 Hz, 3-CH), 123.5 (d, $^4J_{PC}$ = 4.1 Hz, 6-CH), 63.3 (d, $^2J_{PC}$ = 6.0 Hz, PO*CH*$_2$CH$_3$), 16.4 (d, $^3J_{PC}$ = 6.0 Hz, POCH$_2$*CH*$_3$).

^{31}P{^{1}H} NMR ($CDCl_3$): 10.7 (s)

HRMS (APCI) $[M+H]^+$: m/Z calculated for $C_{18}N_2P_2O_6H_{27}^+$: 429.1344; found: 429.1339

Preparation of 4,4′-bipyridine 2,2′-diphosphonic acid (H_4BipyDP).

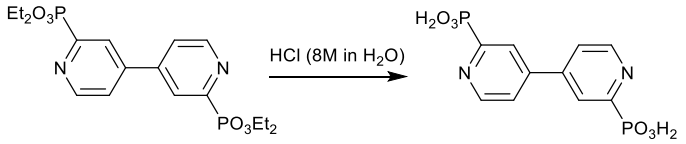

A solution of 3.5 g of **2** in 100 mL of concentrated HCl (35%) and 100 mL of water was stirred overnight at 80°C. The reaction mixture was cooled down and evaporated to dryness. The formed precipitate was collected by centrifugation, washed three times with methanol, and dried in vacuum. Product was obtained as white solid

Yield: 2.2 g (85%)

^{1}H NMR (0.5M KOH in D_2O): 8.62 (m, 1H, 6-*CH*), 8.16 (m, 1H, 3-*CH*), 7.90 (m, 1H, 5-*CH*)

^{13}C{^{1}H} NMR (0.5M KOH in D_2O): 158.2 (d, $^1J_{PC}$ = 182.9 Hz, 2-C), 148.8 (d, $^3J_{PC}$ = 9.7 Hz, 4-C), 146.2 (d, $^3J_{PC}$ = 14.0 Hz, 6-CH), 125.4 (d, $^2J_{PC}$ = 17.0 Hz, 3-CH), 123.9 (s, 5-CH)

^{31}P{^{1}H} NMR (0.5M KOH in D_2O): 3.1 (s)

HRMS (APCI) $[M+H]^+$: m/Z calculated for $C_{10}N_2P_2O_6H_{11}^+$: 317.0092; found: 317.0081

Elemental analysis (wt.%) calculated for $C_{10}H_{10}N_2P_2O_6$ (316.14): C 37.99, H 3.19, N 8.86; found: C 37.73, H 3.28, N 8.60.

Preparation of 4,4′-bipyridine-2,2′-bis(diethoxyphosphonyl)-N,N′-Dioxide (3):

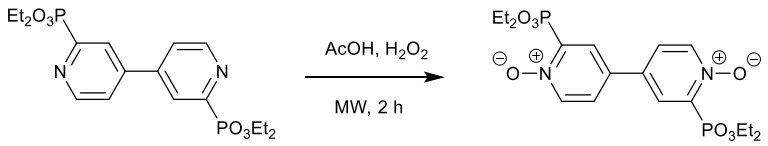

A microwave reaction tube was charged with **2** (0.2 g, 0.466 mmol), 3.6 mL of acetic acid, and 0.7 mL hydrogen peroxide and the mixture was placed into a microwave synthesizer (CEM Discover SP) and reacted at 80 °C for 2 h. The resulting solution was cooled down to RT and evaporated to dryness to remove residual acetic acid. The product was precipitated out with acetone (approximately 50 mL), filtered and dried in vacuum. Product was obtained as white solid.

NOTE: Performing the reaction on large scale did not provide product of sufficient purity, thus the process was repeated multiple times to obtain enough product for a further reaction.

Yield: 75 mg (37%)

^{1}H NMR (D_2O, 600 MHz): 8.34 (dd, $^{3}J_{HH}$ = 6.8 Hz, $^{4}J_{PH}$ = 4.4 Hz, 1H, 6-*CH*), 8.14 (dt, $^{3}J_{PH}$ = 10.3 Hz, $^{4}J_{HH}$ = 2.5 Hz, 1H, 3-*CH*), 7.95 (dd, $^{3}J_{HH}$ = 6.8 Hz, $^{4}J_{HH}$ = 2.5 Hz, 5-*CH*), 4.20 (m, 4H, PO*CH*$_2$CH$_3$), 1.22 (t, $^{3}J_{HH}$ = 7.2 Hz, 6H, POCH$_2$*CH*$_3$)

^{13}C{^{1}H} NMR (D_2O, 151 MHz): 140.9 (d, $^{3}J_{PC}$ = 6.4 Hz, 6-CH), 140.0 (d, $^{1}J_{PC}$ = 218.1, 2-C), 136.1 (d, $^{3}J_{PC}$= 11.4 Hz, 4-C), 130.3 (d, $^{2}J_{PC}$ = 11.6 Hz, 3-CH), 128.1 (s, 5-CH), 65.8 (d, $^{2}J_{PC}$ = 6.3 Hz, PO*CH*$_2$CH$_3$), 15.6 (d, $^{3}J_{PC}$ = 5.7 Hz, POCH$_2$*CH*$_3$)

^{31}P{^{1}H} NMR (D_2O, 243 MHz): 6.0 (s)

HRMS (APCI) $[M+H]^+$: m/Z calculated for $C_{18}N_2P_2O_8H_{27}^+$: 461.1243; found: 461.1237

Preparation of octaethyl 4,4′-bipyridine-2,2′,6,6′-tetraphosphonate (4):

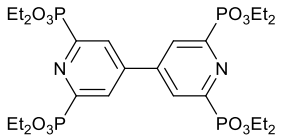

A Schlenk tube was charged with 160 mg of **3** (0.373 mmol) and acetonitrile (approx. 50 mL) was added under argon atmosphere. The reaction mixture was stirred at RT for 30 min and six equivalents of ethyl chloroformate were added dropwise (0.20 mL, 2.1 mmol). After 1 h upon stirring at RT, six equivalents of triethyl phosphite were added (0.36 mL, 2.1 mmol) and the reaction was stirred for another 72 h. The reaction mixture was evaporated to dryness, diluted by water, and extracted three times with dichloromethane. The combined organic phase was dried over a large amount of Na_2SO_4 and evaporated to dryness. The product was purified by column chromatography on neutral aluminium oxide. First, pure dichloromethane was used to wash out the impurities and afterwards the product was eluted by a 9:1 to 8:2 dichloromethane/methanol mixture. Product was obtained as white solid. According to the NMR analysis, the product ca 5% of impurities, these do not interfere in further reactivity and were removed in the subsequent reaction step.

Yield: 180 mg (73%)

^{1}H NMR ($CDCl_3$, 600 MHz): 8.26 (m, 1H, CH^{Ar}), 4.29 (m, 4H, $POCH_2CH_3$), 1.38 (m, 6H, $POCH_2CH_3$)

^{13}C{^{1}H} NMR ($CDCl_3$): 155.4 (dd, $^1J_{PC}$ = 226.1 Hz, $^3J_{PC}$ = 22.5 Hz, 2,6-C), 144.6 (t, $^3J_{PC}$= 11.8 Hz, 4-C), 127.1 (dd, $^2J_{PC}$ = 25.5. Hz, $^4J_{PC}$ = 3.8 Hz, 3,5-CH), 63.5 (d, $^2J_{PC}$ = 6.1 Hz, $POCH_2CH_3$), 16.1 (d, $^2J_{PC}$ = 6.1 Hz, $POCH_2CH_3$)

^{31}P{^{1}H} NMR ($CDCl_3$): 8.7 (s)

HRMS (APCI) $[M+H]^+$: m/Z calculated for $C_{26}N_2P_4O_{12}H_{45}^+$: 701.1923; found: 701.1917

Preparation of 4,4′-bipyridine-2,2′,6,6′-tetraphosphonic acid (H_8BipyTP):

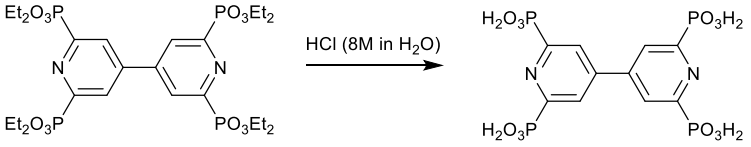

A round bottom flask was charged with 200 mg of **4**, 7.5 mL of concentrated HCl, and 3.5 mL of water. The solution was heated overnight at 80 °C. After cooling down, the reaction mixture was evaporated to dryness, washed with methanol, centrifuged (the process was repeated three times) and dried in vacuum. Product was obtained as white solid.

Yield: 90 mg (74%)

^{1}H NMR (D_2O): 7.82 (br, 3,5-*CH*)

^{13}C{^{1}H} NMR (D_2O): 157.1 (dd, $^1J_{PC}$ = 192.8 Hz, $^3J_{PC}$ = 14.5 Hz, 2,6-C), 147.9 (t, $^3J_{PC}$= 10.8 Hz, 4-C), 125.8 (dd, $^2J_{PC}$ = 25.5. Hz, $^4J_{PC}$ = 3.8 Hz, 3,5-CH)

^{31}P{^{1}H} NMR (D_2O): 1.6 (s)

Elemental analysis (wt.%) calculated for $C_{10}H_{12}N_2P_4O_{12}$ (476.10): C 25.23, H 2.54, N 5.88; found: C 23.60, H 3.16, N 5.53.

Instrumental methods

NMR spectra were recorded on JEOL Delta 600 spectrometer at 20 °C with resonance frequencies of 600 MHz for ^{1}H, 151 MHz for ^{13}C, and 243 MHz for ^{31}P. ^{1}H and ^{13}C NMR chemical shifts (δ in ppm) are given relative to TMS and referenced to the residue solvent signal ($CDCl_3$: δ_H = 7.26, δ_C

= 77.0, D2O: δ_H = 4.79). ^{13}C measurements in D_2O and ^{31}P signals were referenced to the primary standard of the unified chemical shift scale in accordance with IUPAC recommendations [1].

Powder X-ray diffraction (XRD) was measured using a PANalytical X'Pert PRO diffractometer in reflection geometry equipped with a conventional Co X-ray tube (40 kV, 30 mA). Qualitative analysis was performed with the HighScorePlus software package (PANalytical, Almelo, The Netherlands, version 3.0).

Fourier transform infrared (FTIR) spectra were collected with a Nicolet NEXUS 670-FT spectrometer (Thermo Fisher Scientific, Waltham, MA, USA) with an ATR accessory. Thermal analyses (DTA/TGA) were carried out on a Setaram SETSYS Evolution-16-MS (Setaram, Caluire, France) instrument coupled with a mass spectrometer for the detection of evolved gases. The measurements were performed in the flow of synthetic air (60 mL min^{-1}) from 25 to 1000 °C with a heating rate of 10 °C min^{-1}. DSC analysis was performed on DSC 821e Mettler Toledo (Mettler-Toledo, Greifensee, Switzerland) coupled with an intercooler. All measurements were under a nitrogen atmosphere with a flow rate of 50 mL min^{-1}. Each sample was heated from –20 to 150 °C at a heating rate of 5 °C min^{-1}, cooled down to –20 °C and again heated up to 150 °C.

Chemical analytical data for the organic precursors

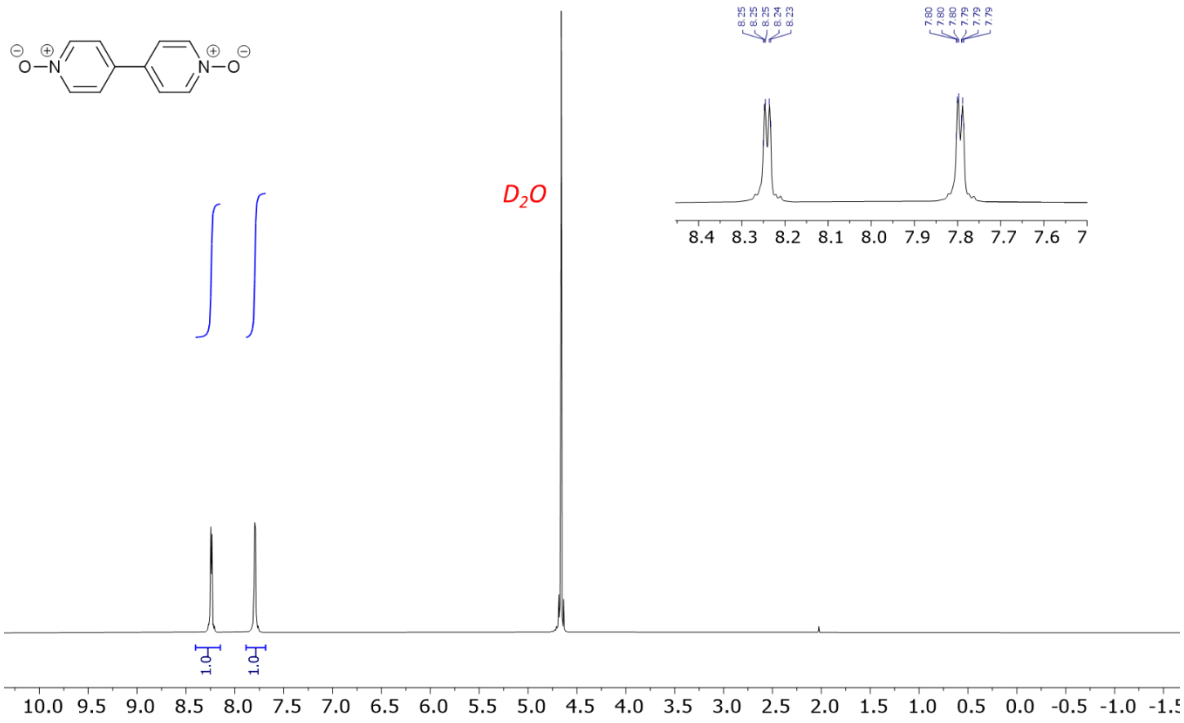

Figure S1: ^{1}H NMR (D_2O) spectrum of **1**.

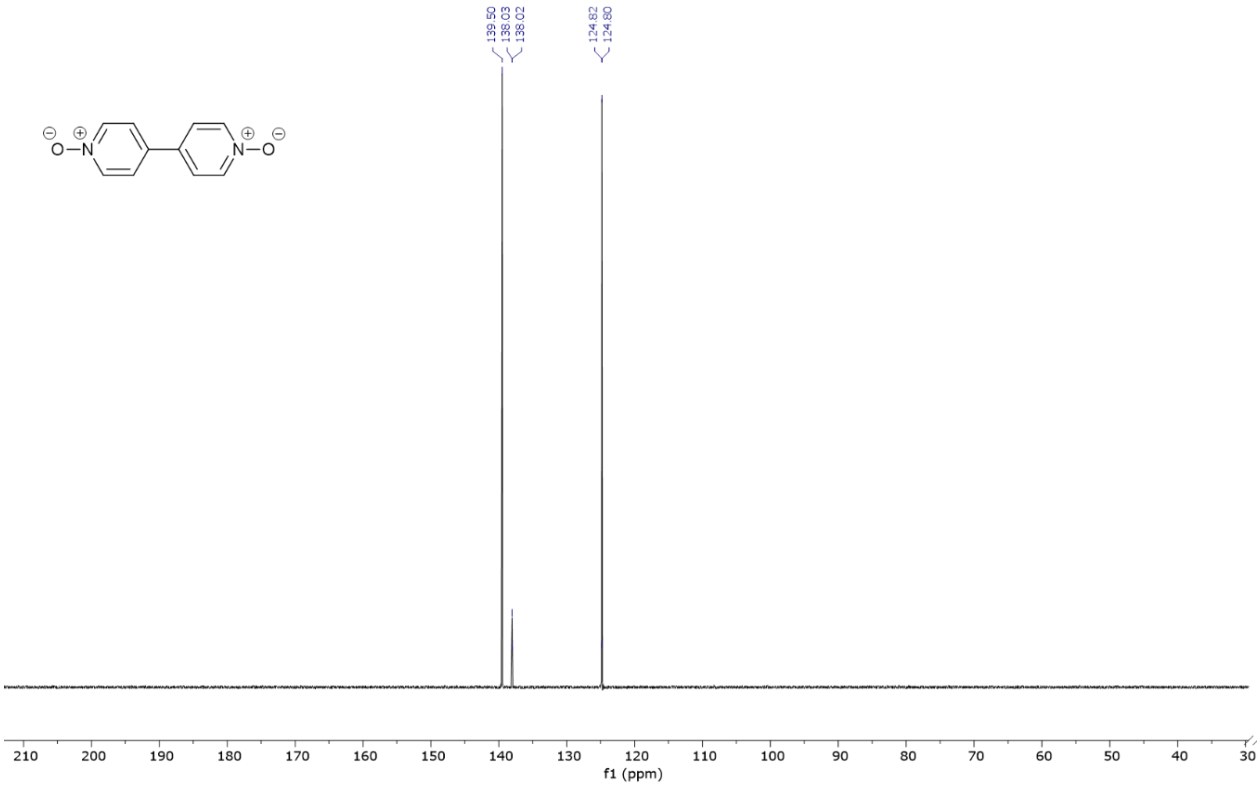

Figure S2: $^{13}C\{^{1}H\}$ NMR ($CDCl_3$) spectrum of **1**.

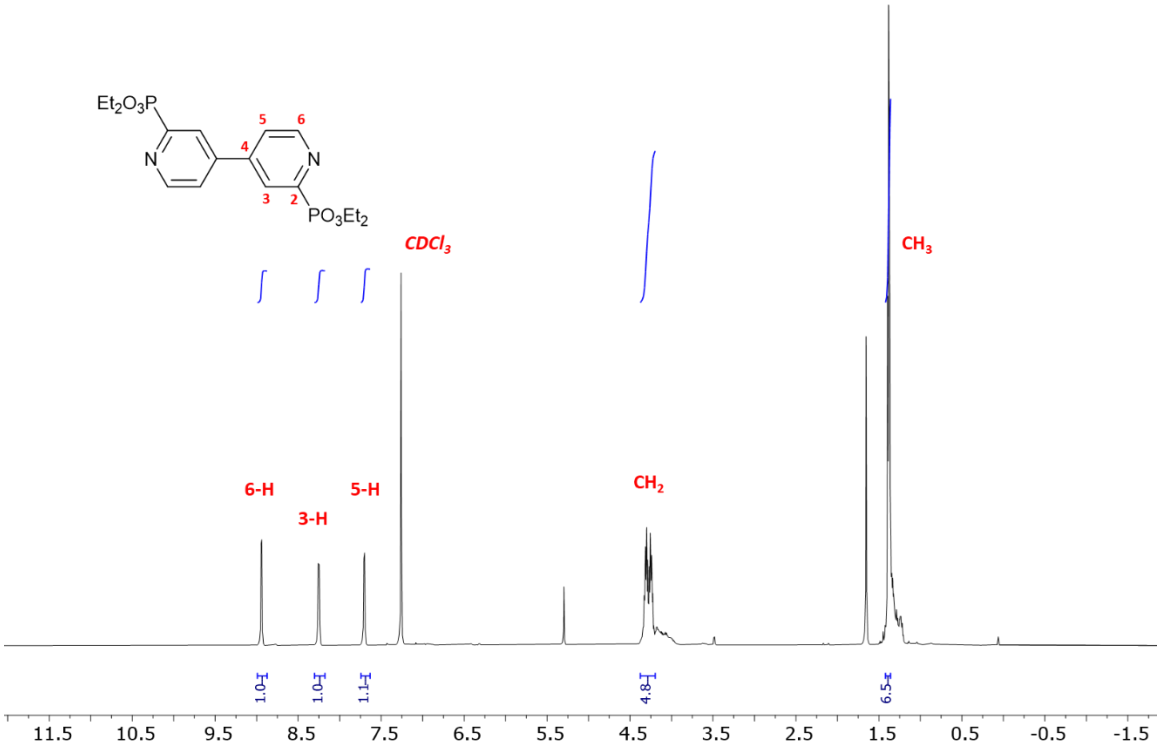

Figure S3: ^{1}H NMR ($CDCl_3$) spectrum of **2**.

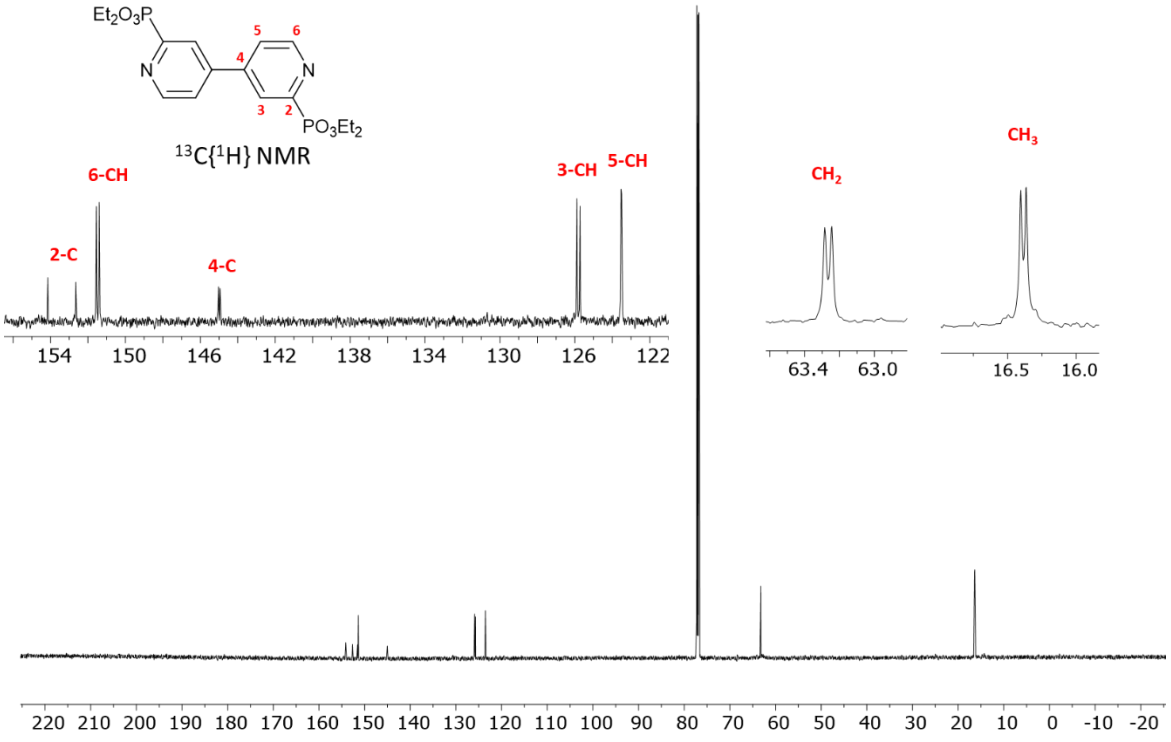

Figure S4: $^{13}C\{^{1}H\}$ NMR ($CDCl_3$) spectrum of **2**.

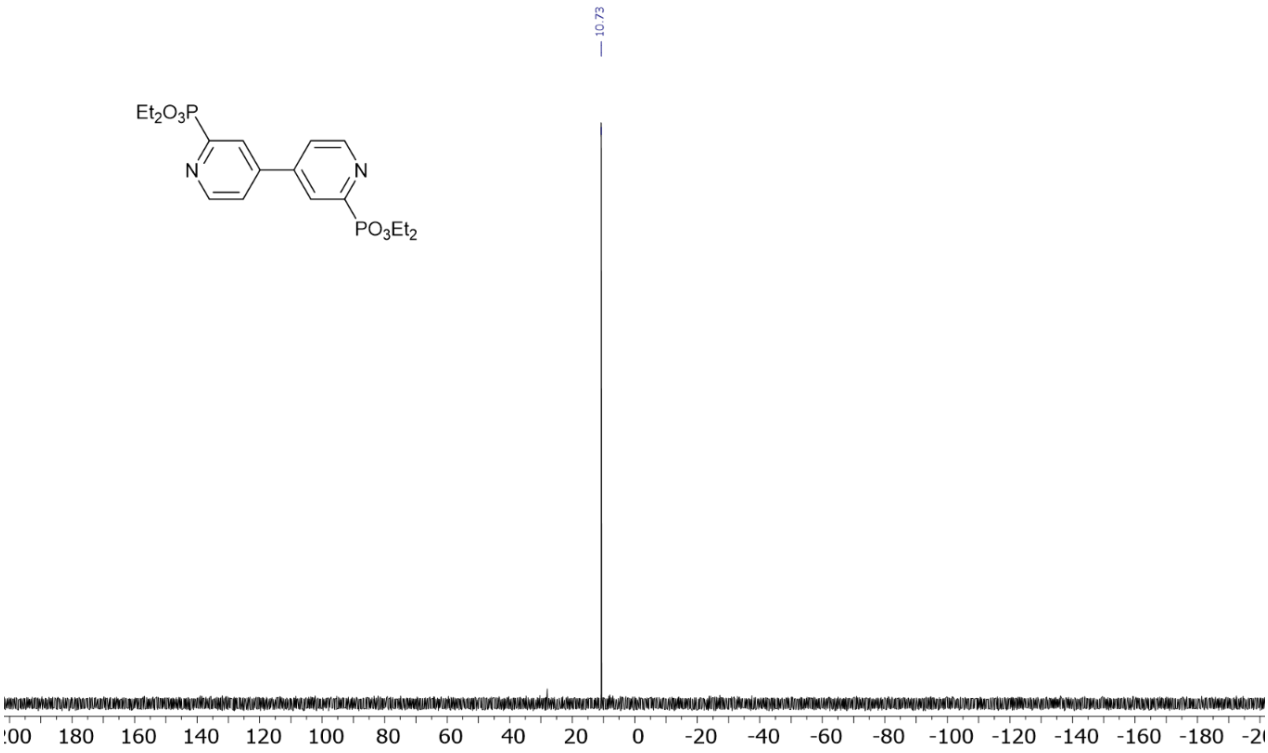

Figure S5: $^{31}P\{^{1}H\}$ NMR ($CDCl_3$) spectrum of **2**.

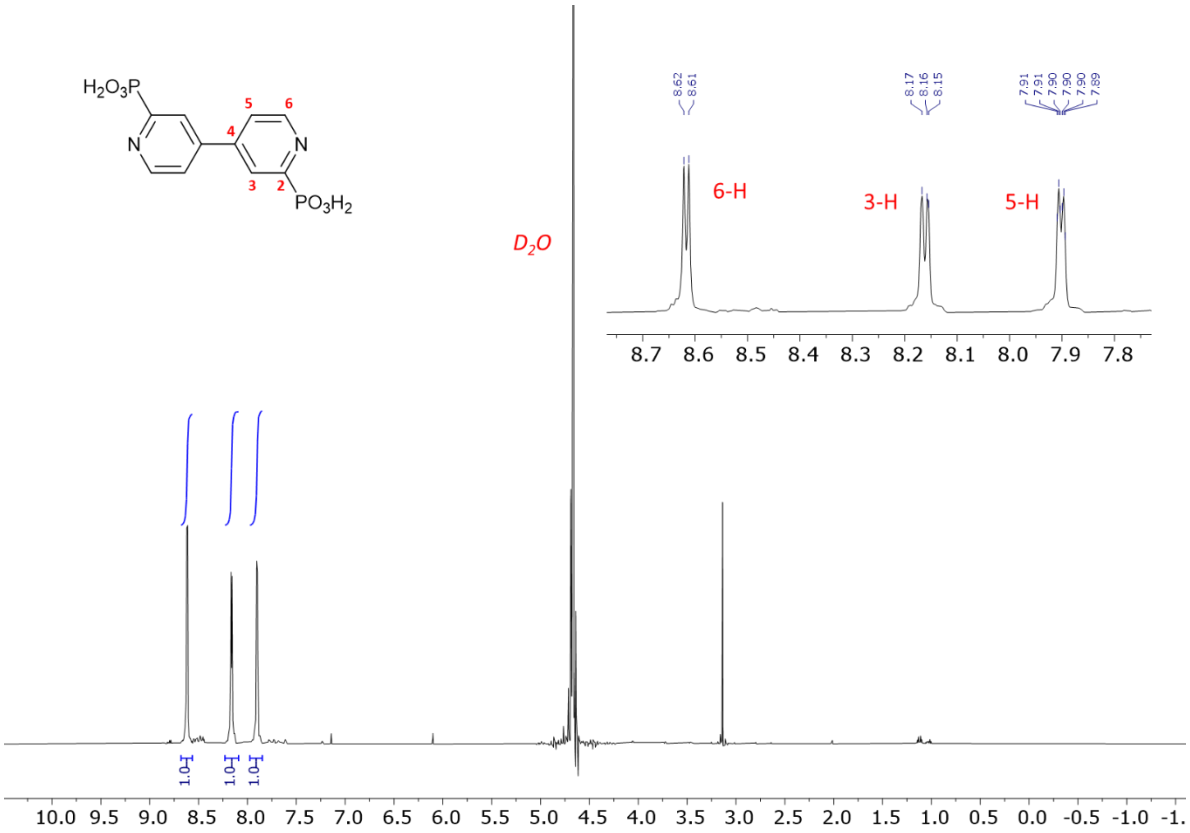

Figure S6: ^{1}H NMR (D_2O) spectrum of **H_4BipyDP**.

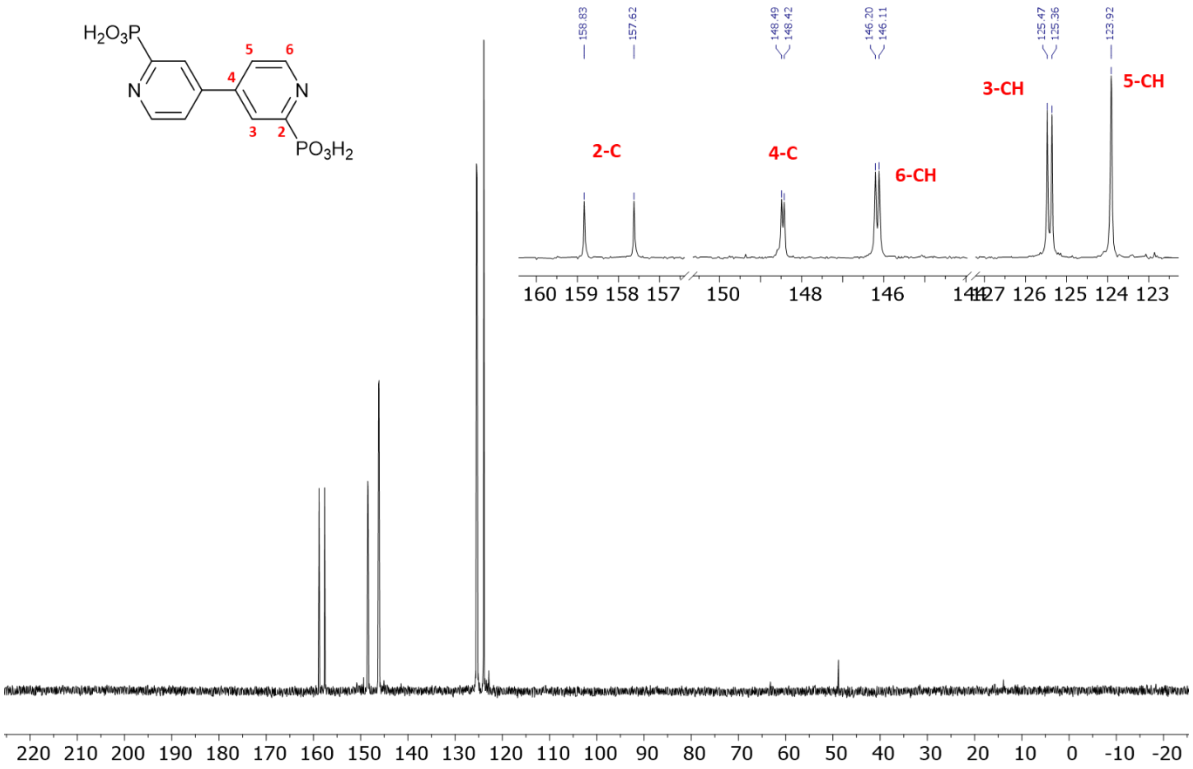

Figure S7: $^{13}C\{^{1}H\}$ NMR (D_2O) spectrum of **H_4BipyDP**.

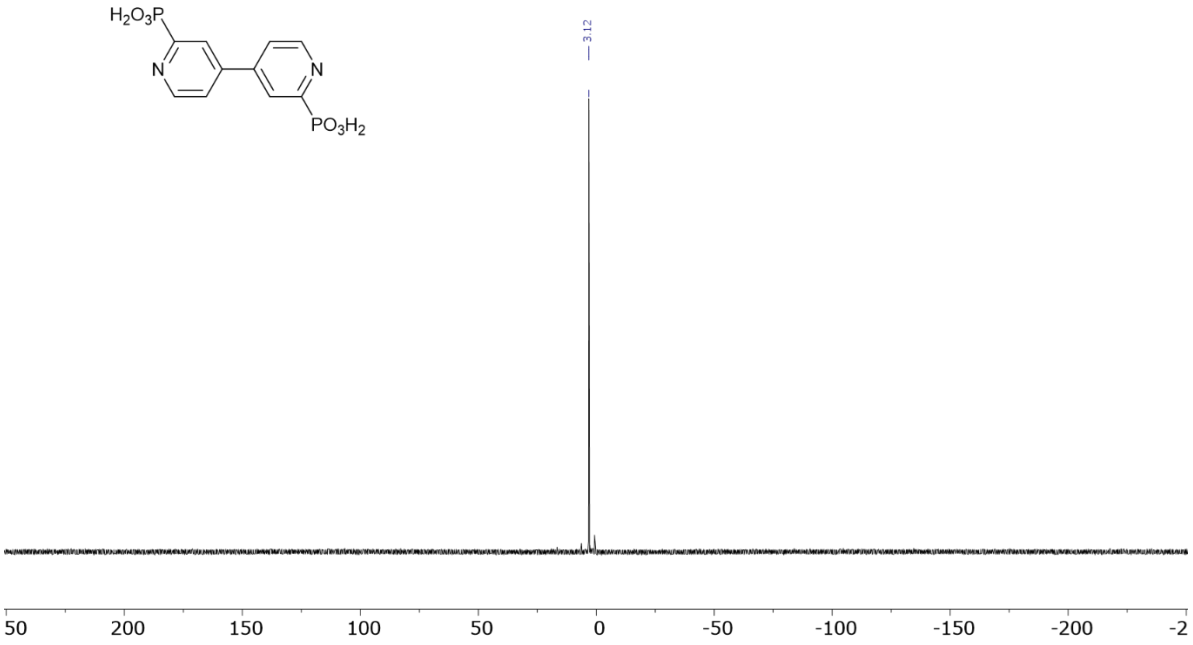

Figure S8: $^{31}P\{^{1}H\}$ NMR spectrum of **H_4BipyDP**.

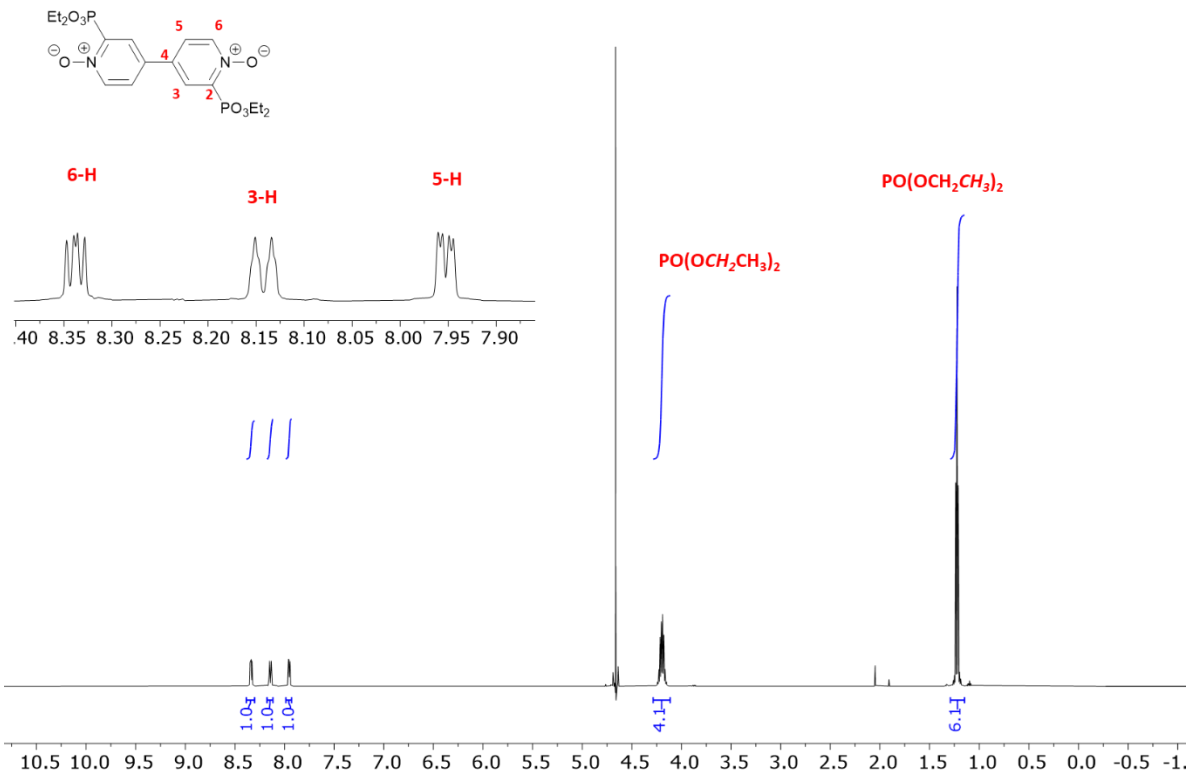

Figure S9: ^{1}H NMR (D_2O) spectrum of **3**.

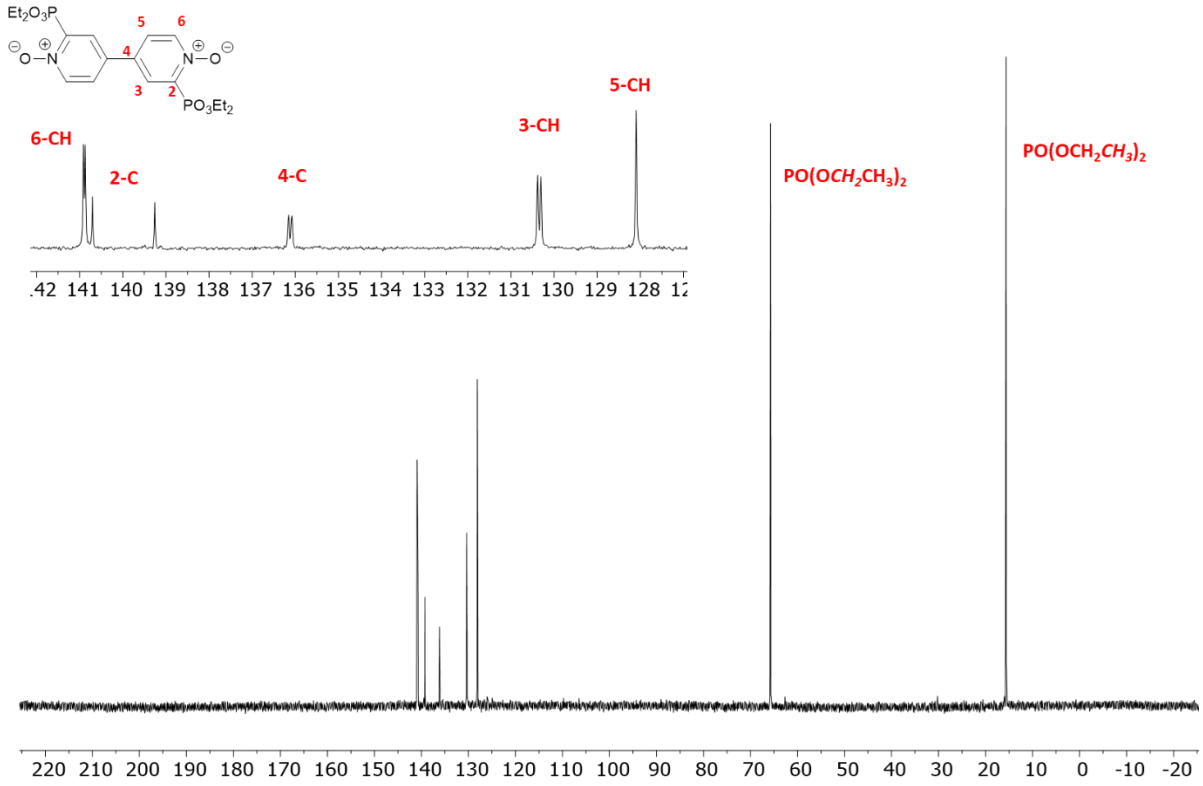

Figure S10: $^{13}C\{^{1}H\}$ NMR (D_2O) spectrum of **3**.

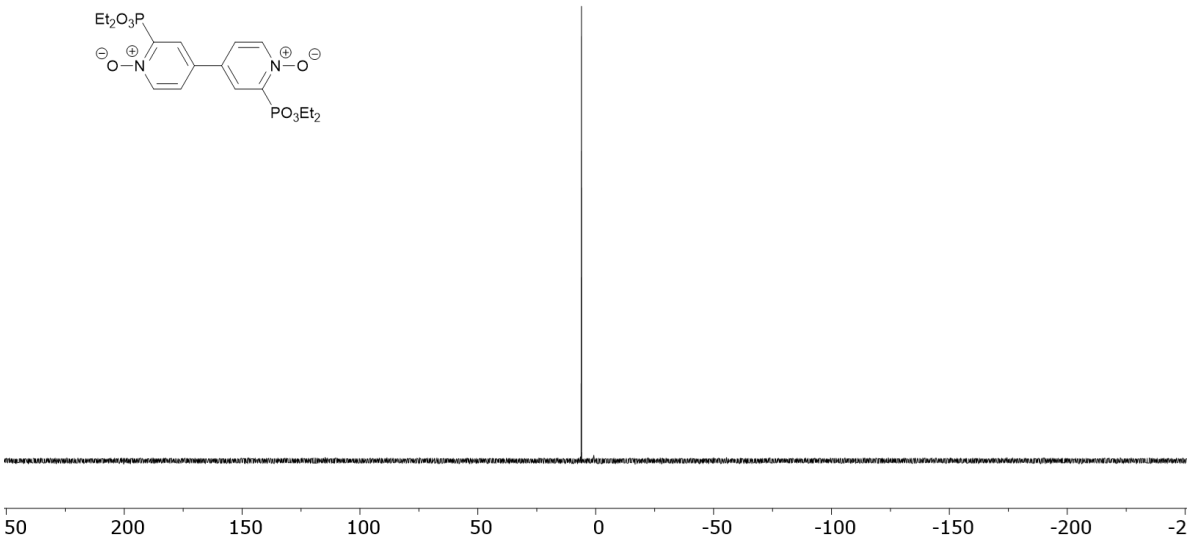

Figure S11: $^{31}P\{^{1}H\}$ NMR (D_2O) spectrum of **3**.

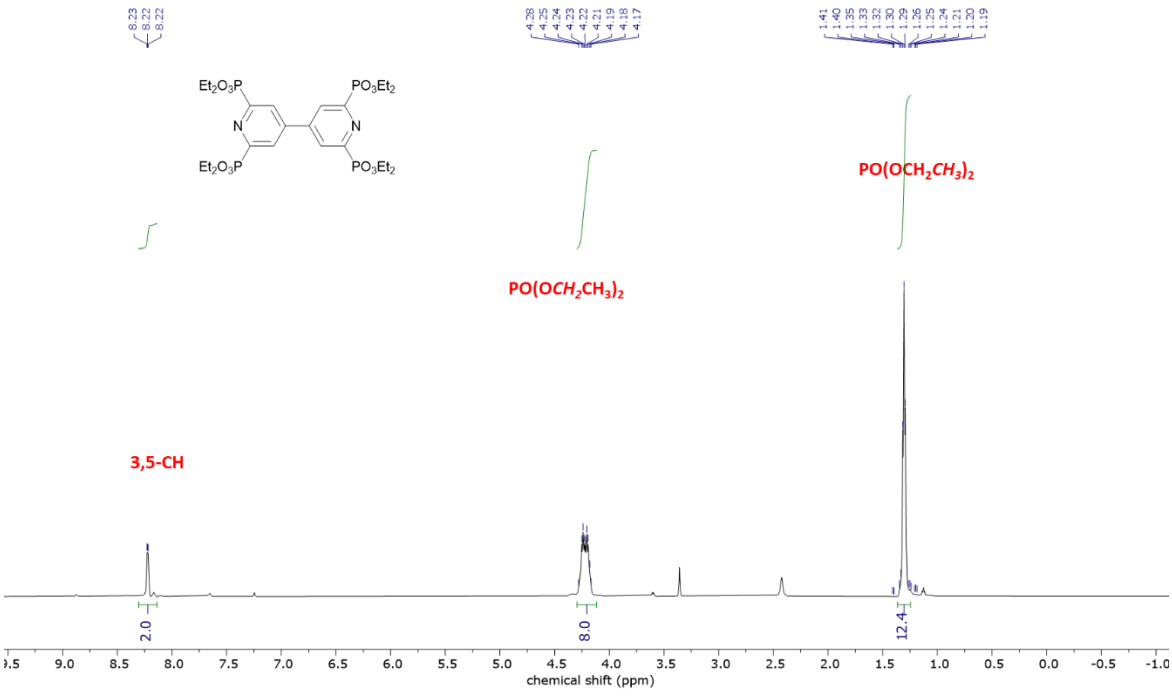

Figure S12: ^{1}H NMR ($CDCl_3$) spectrum of **4**.

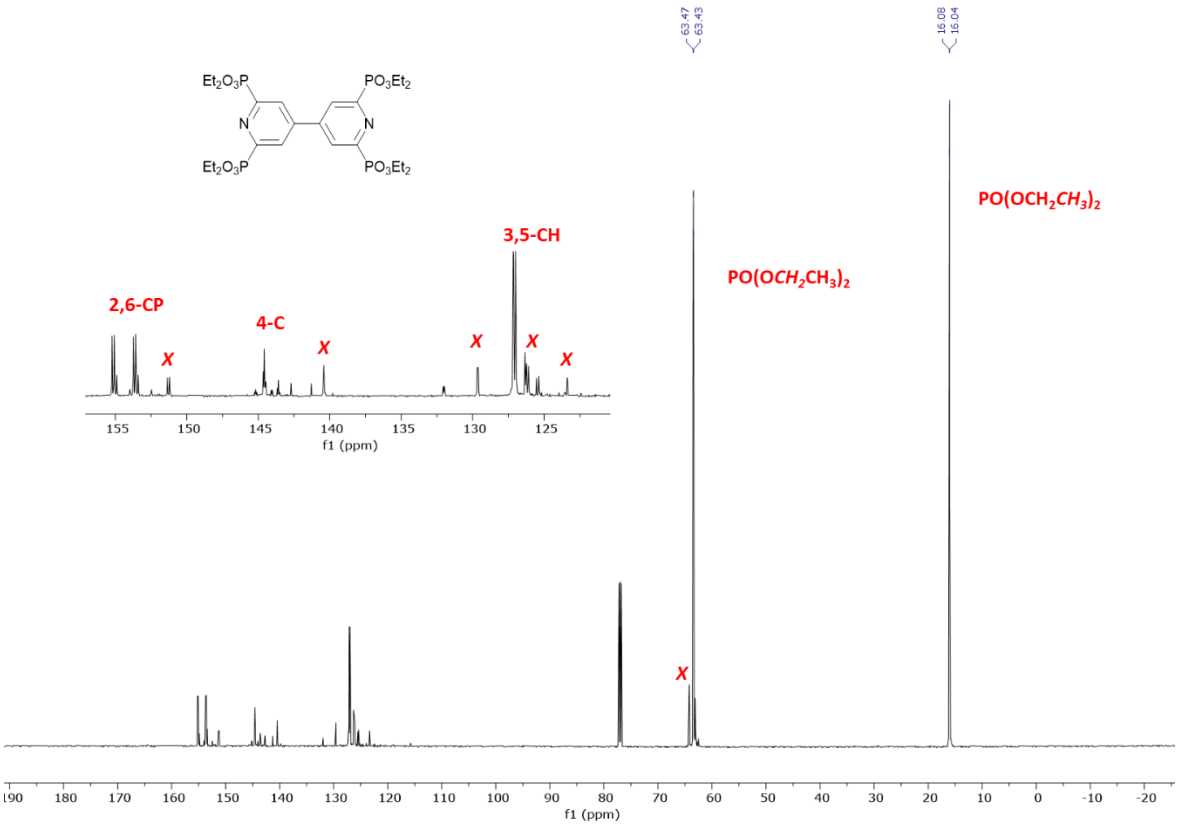

Figure S13: $^{13}C\{^{1}H\}$ NMR ($CDCl_3$) spectrum of **4**(*X* denotes unindentified impurities).

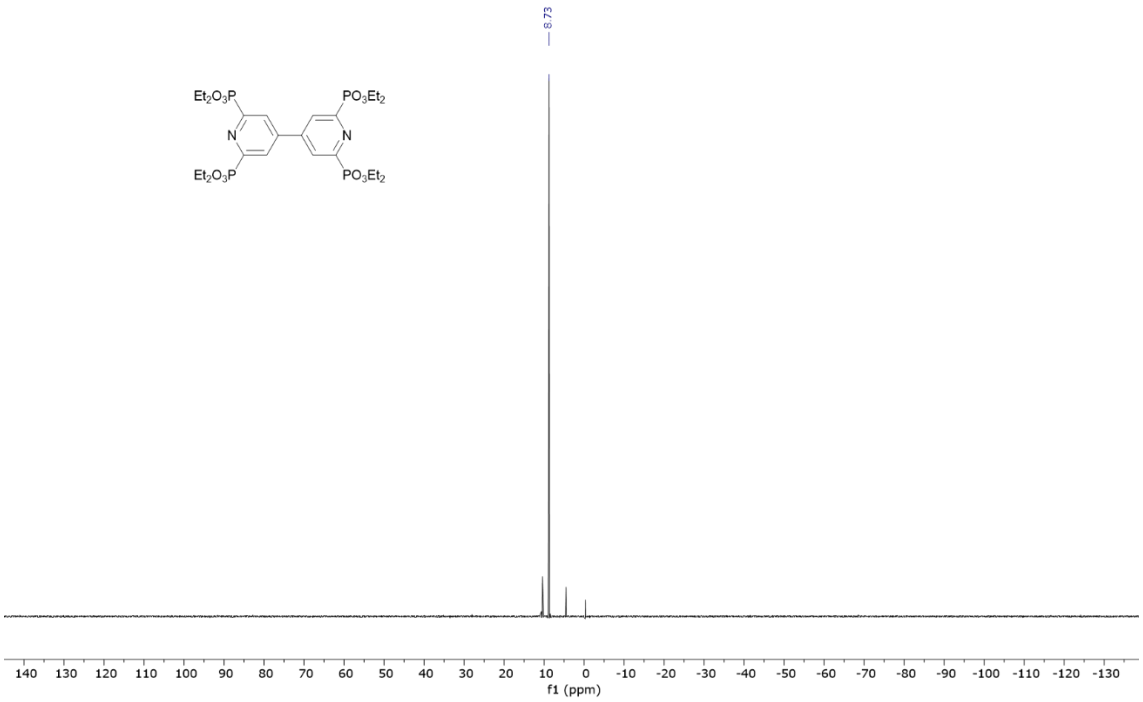

Figure S14: $^{31}P\{^{1}H\}$ NMR spectrum of **4**.

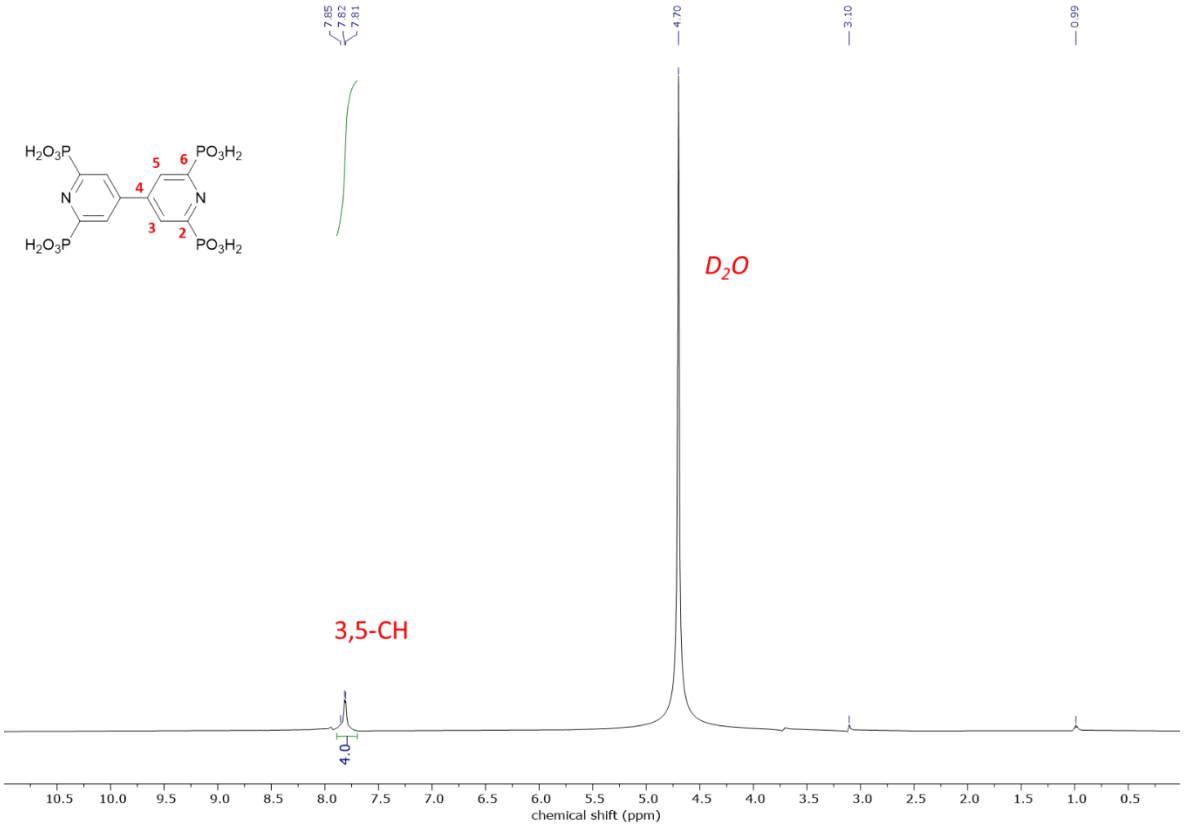

Figure S15: ^{1}H NMR (D_2O) spectrum of **H_8BipyTP**.

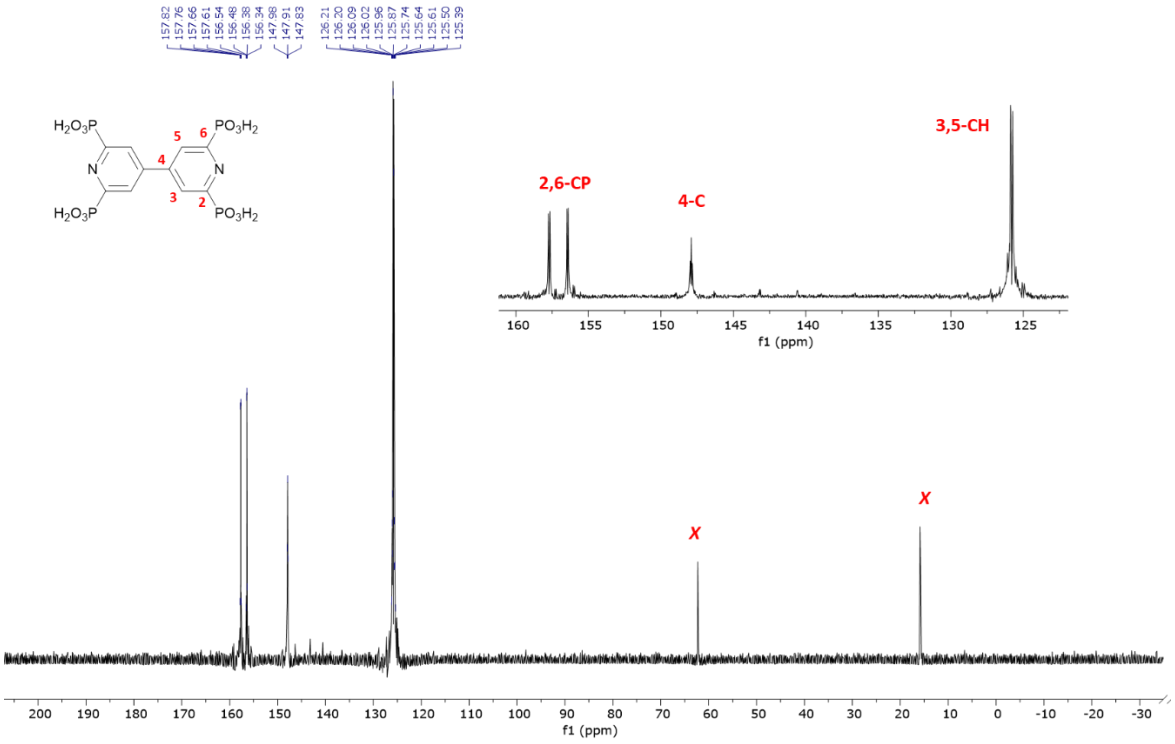

Figure S16: $^{13}C\{^{1}H\}$ NMR (D_2O) spectrum of **H_8BipyTP** (X denotes residual solvent signals).

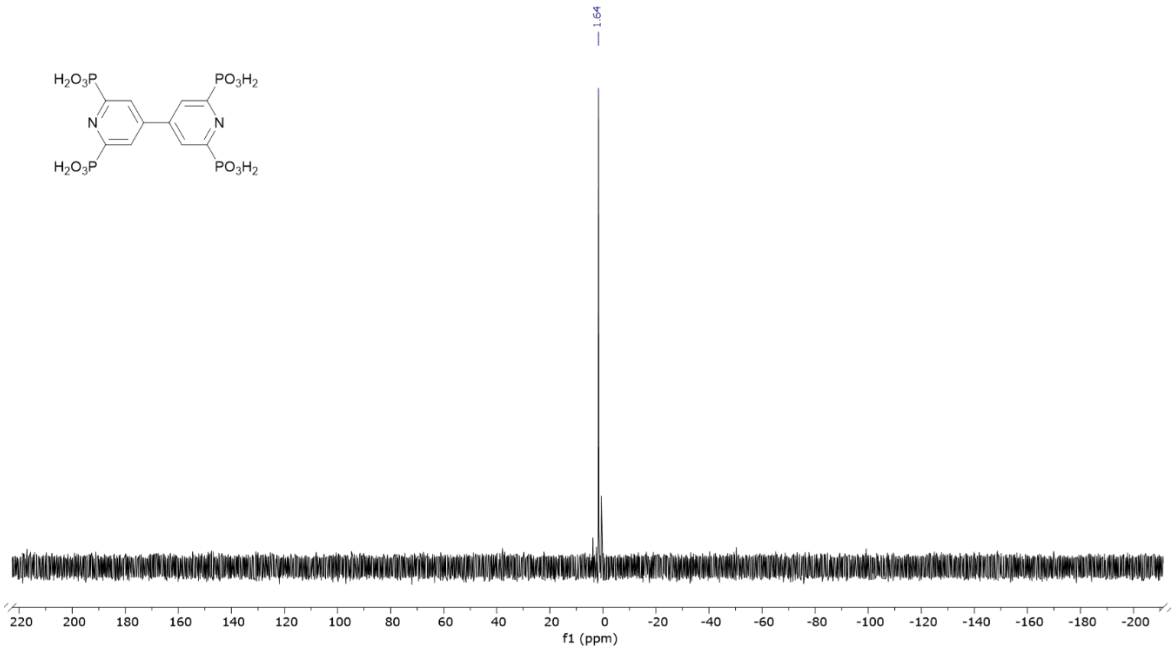

Figure S17: $^{31}P\{^{1}H\}$ NMR (D_2O) spectrum of **H_8BipyTP**.

Characterization of the materials

Structural analysis

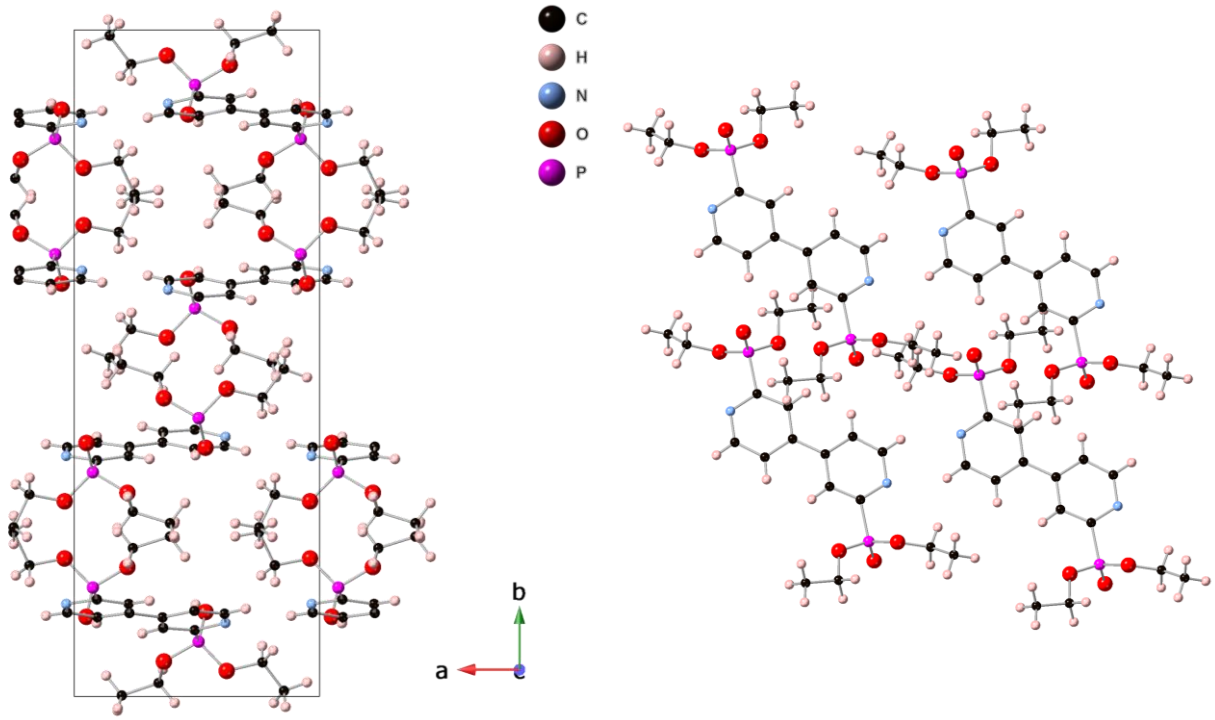

Figure S18: The crystal structure of compound **2** (left) and a detail of one layer (right). Colour coding is as follows: P (magenta), O (red), C (black), N (blue), H (light pink). The compound crystallizes in a monoclinic $P2_1/n$ group. The crystal is composed of layers in the ac plane held by weak C-H···N hydrogen bonds between the 4,4′-bipyridine moieties with the two phosphonate groups pointing to either side of the 4,4′-bipyridine skeleton. Individual layers interact with each other via van der Waals forces mediated by ethyl groups bonded to the oxygen atoms.

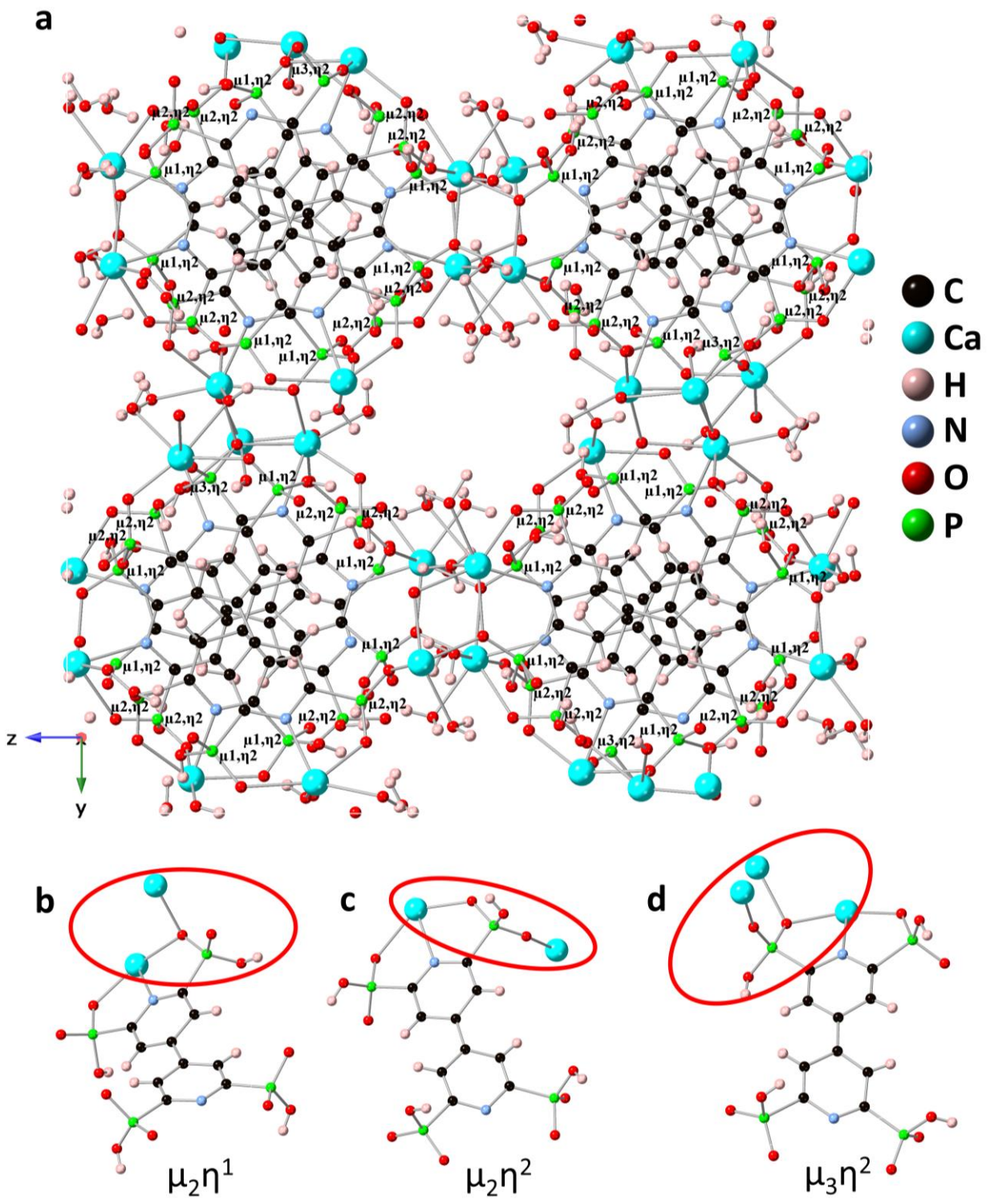

Figure S19: (a) Assignment of the coordination modes of phosphonate groups in the crystal structure of ICR-25. Detailed views of the BipyTP^{8-} linker coordinated in (a) μ_2,η^1, (b) μ_2,η^2, and (c) μ_3,η^2 coordination mode.

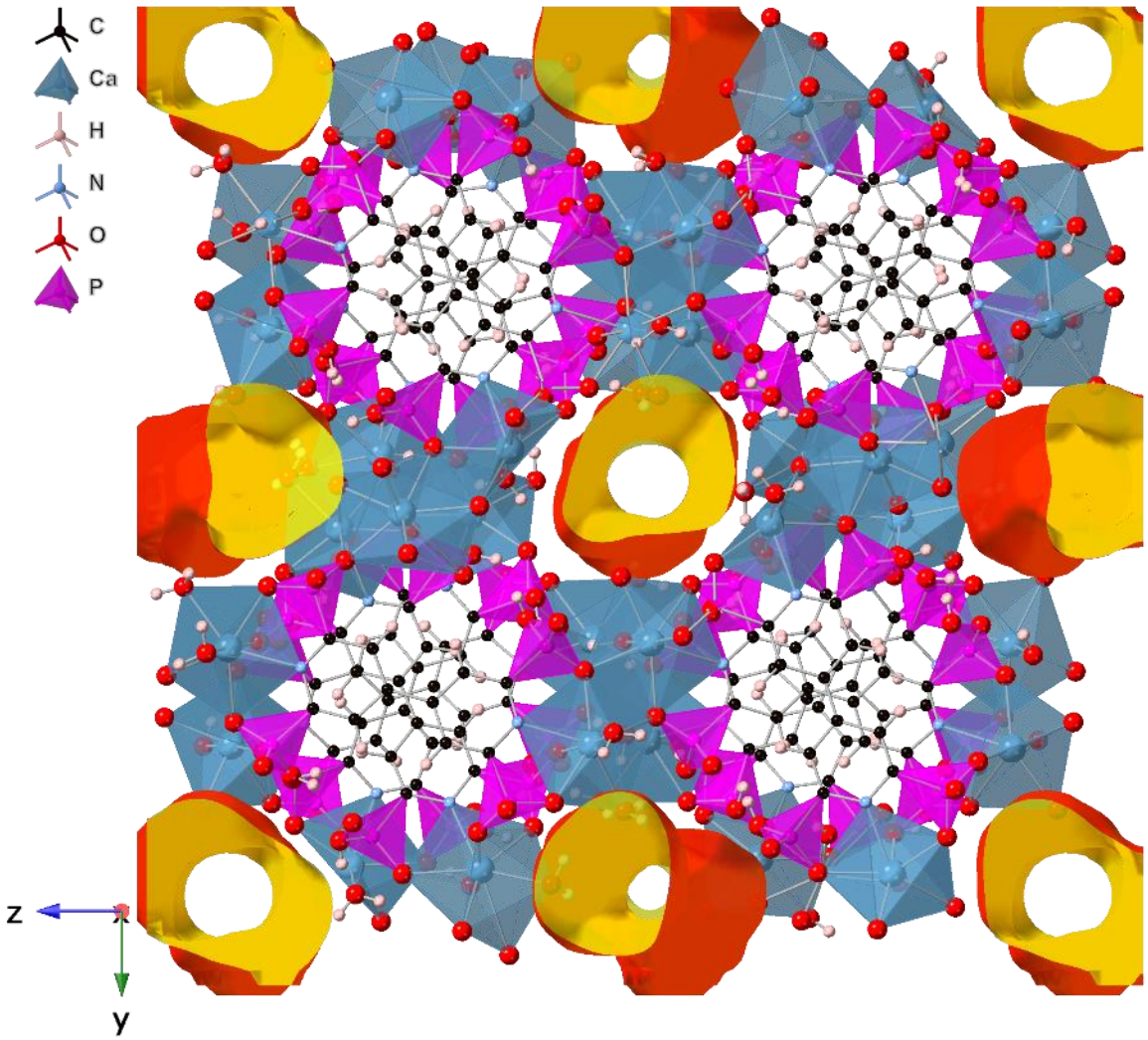

Figure S20: Detail of the ICR-25 structure viewed along the *x*-axis with the visualized potential voids. Colour coding is as follows: phosphonate tetrahedra (magenta), O (red), C (black), N (blue), H (light pink), Ca atoms (cyan), structural voids (yellow).

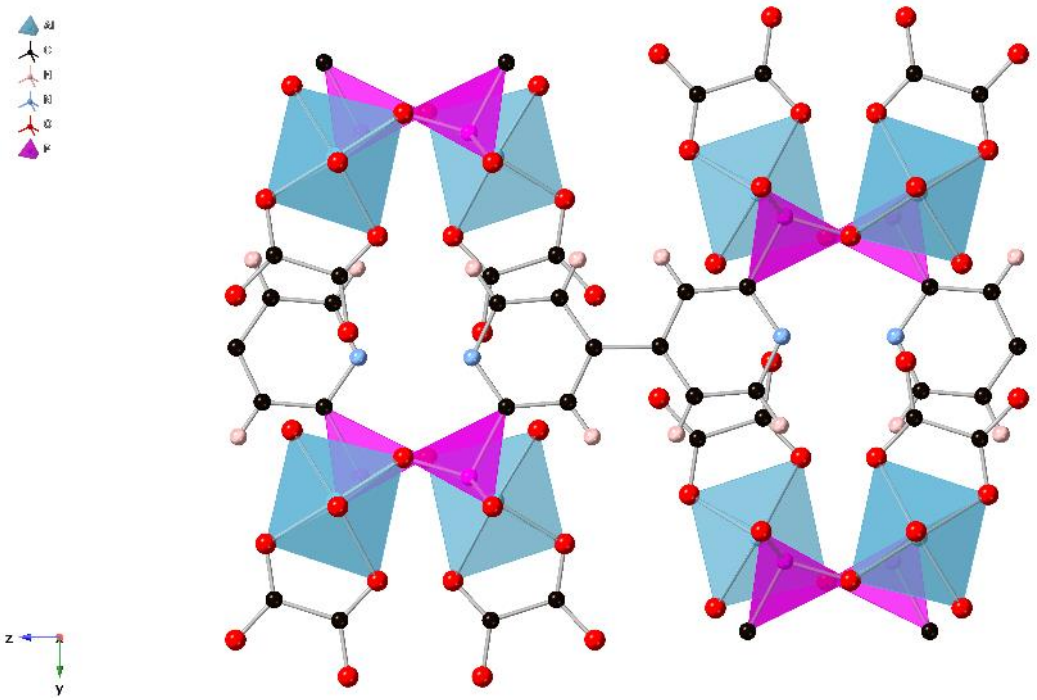

Figure S21: Detail of the ICR-26 structure in the (100) projection showing the coordination of the **BipyDP**$^{4-}$ and oxalate ligands. Colour coding is as follows: phosphonate tetrahedra (magenta), O (red), C (black), N (blue), H (light pink), octahedrally coordinated Al atoms (pastel cyan).

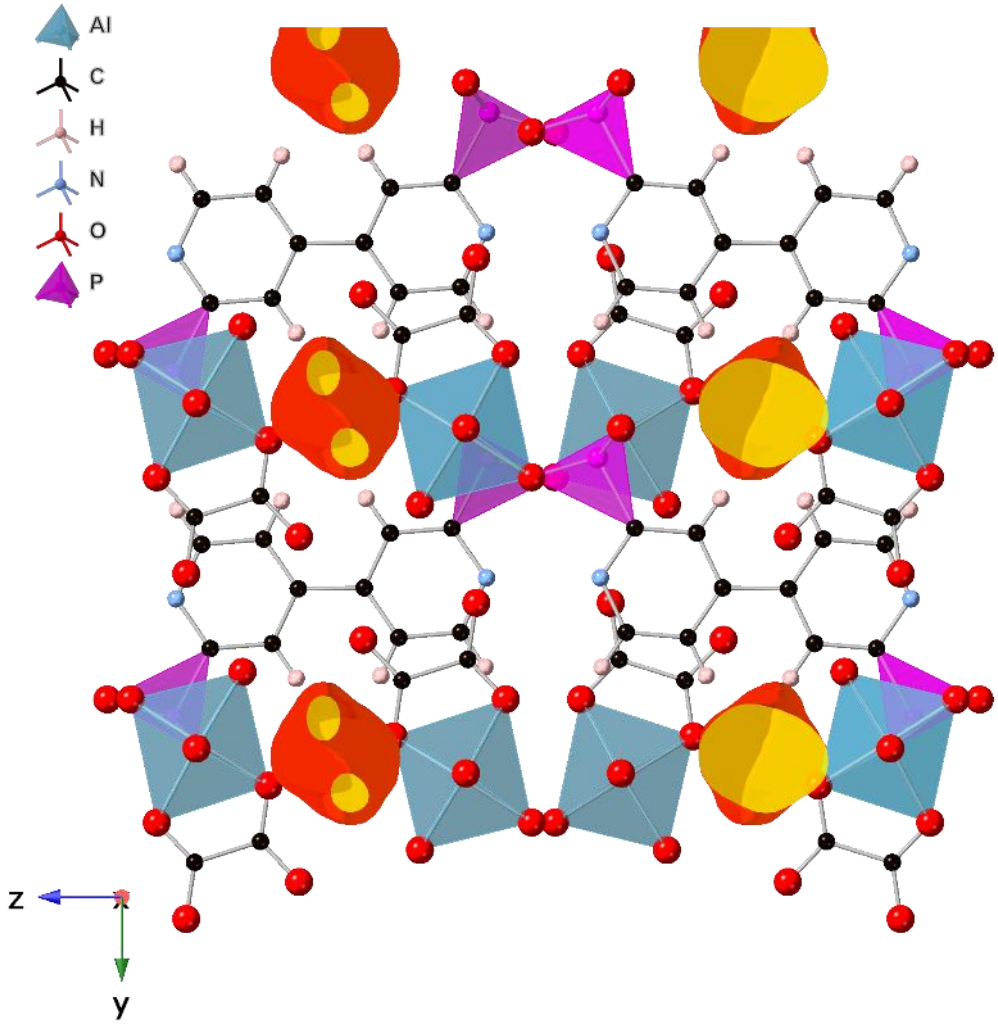

Figure S22: Detail of the ICR-26 structure viewed along the *x*-axis with the visualized potential voids. Colour coding is as follows: phosphonate tetrahedra (magenta), O (red), C (black), N (blue), H (light pink), octahedrally coordinated Al atoms (pastel cyan), structural voids (yellow).

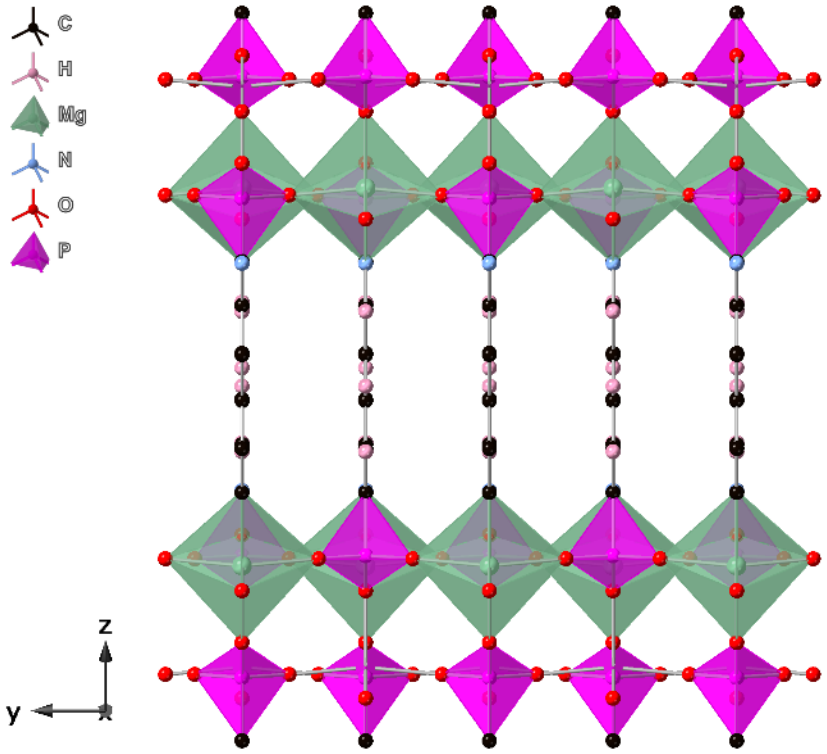

Figure S23: Detail of the ICR-27 structure in the (100) projection showing the layered ordering of the **BipyDP**$^{4-}$ ligands perpendicular to the Mg–O–P–O–Mg bridges. Colour coding is as follows: phosphonate tetrahedra (magenta), O (red), C (black), N (blue), H (light pink), octahedrally coordinated Mg atoms (green).

FTIR analysis of the materials

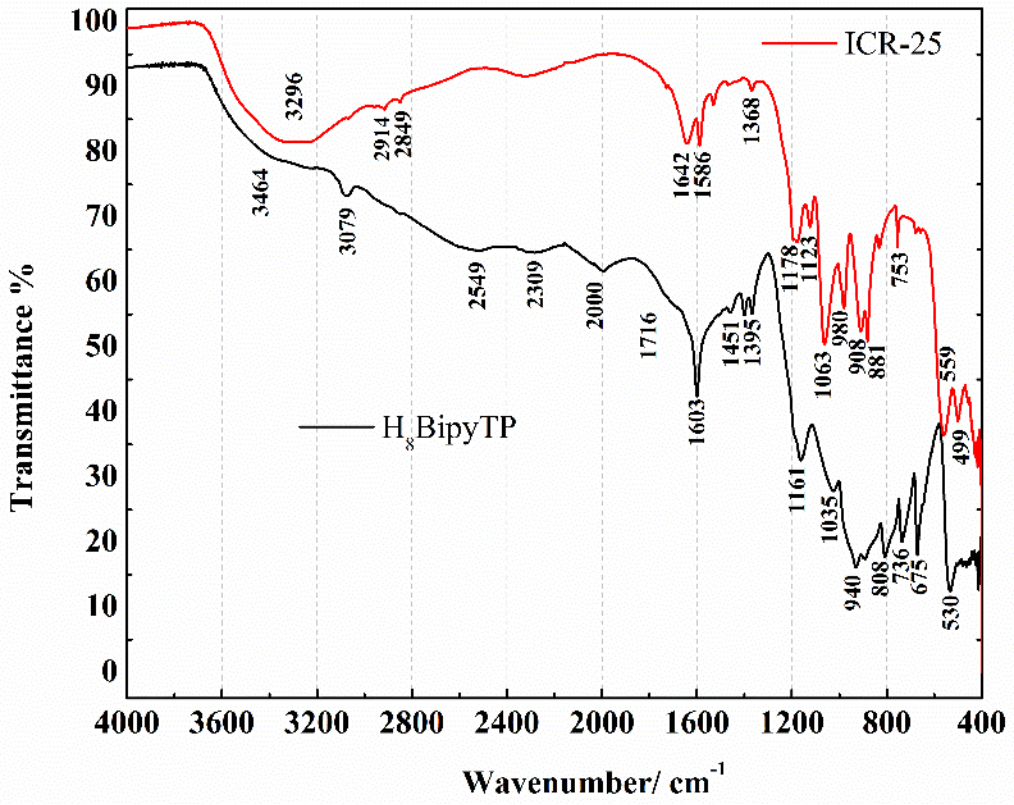

Figure S24: FTIR-Spectrum of **H8BipyTP** linker and ICR-25.

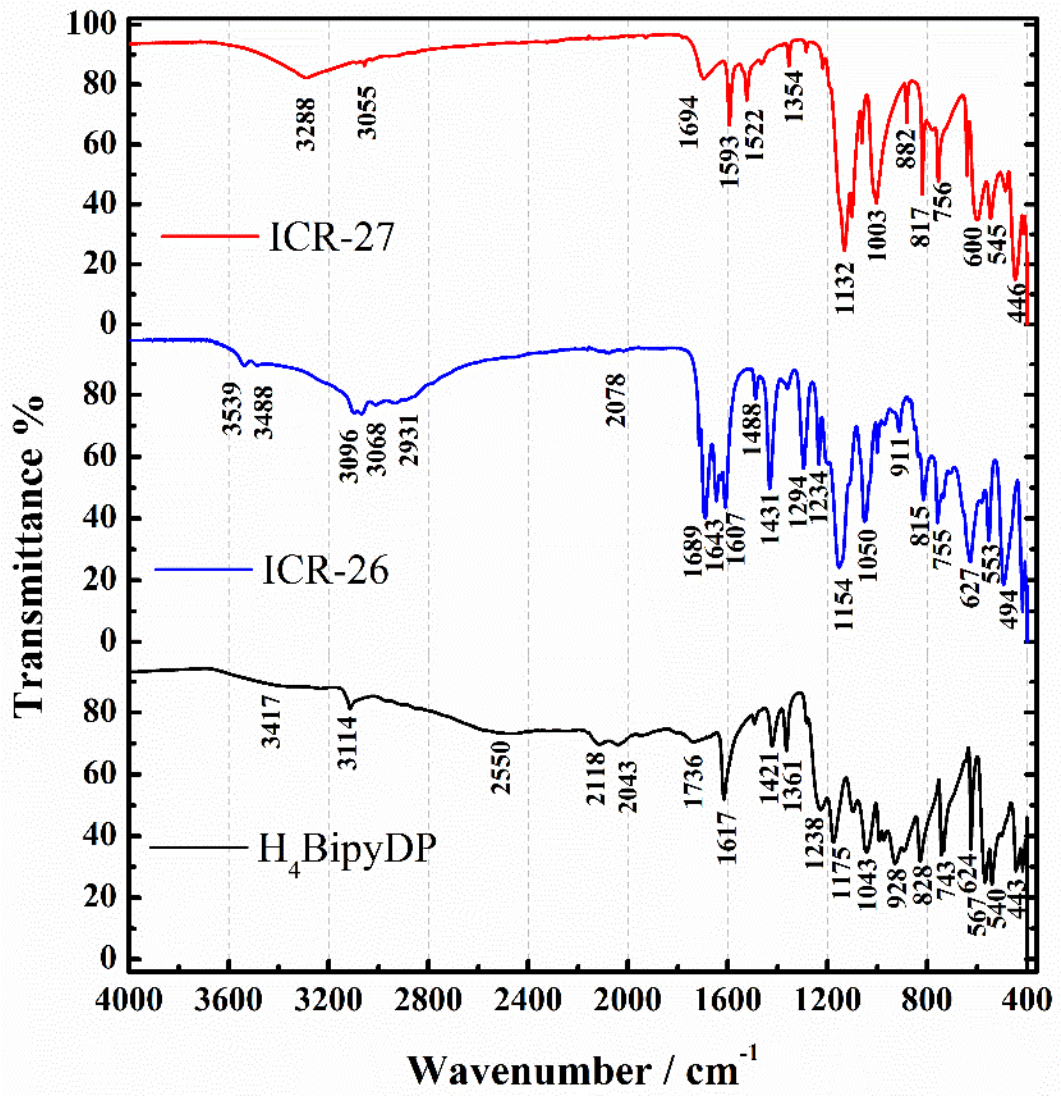

Figure S25: FTIR spectrum of **H_4BipyDP** linker, ICR-26, and ICR-27.

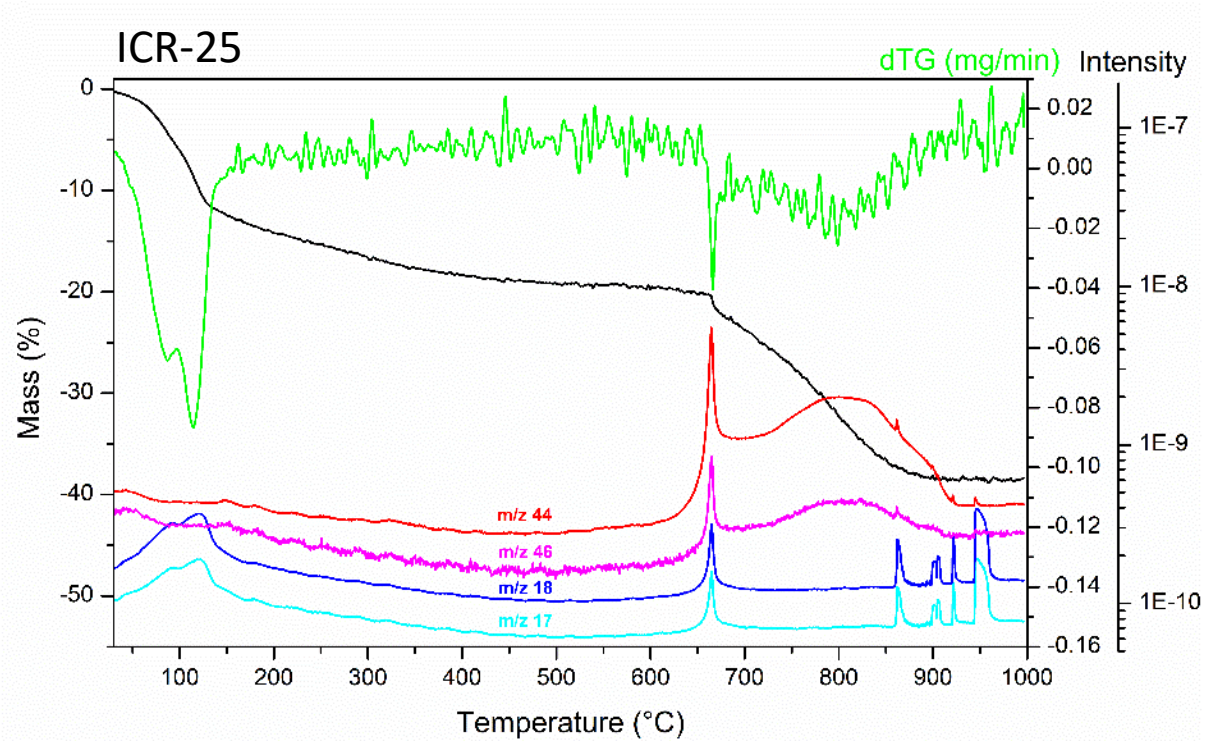

Figure S26: TG/dTG curves and the evolution of gases for ICR-25 on air; m/z = 17 – OH, m/z = 18 – H_2O, m/z = 44 – CO_2, and m/z = 46 – NO_2.

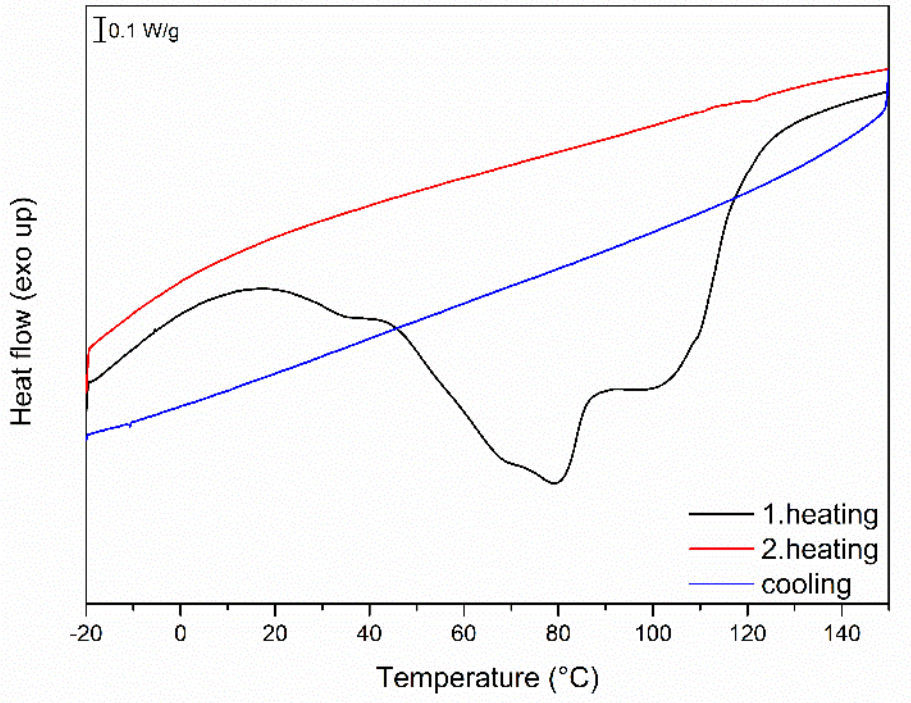

Figure S27: DSC curves showing the first heating, cooling, and repeated heating of ICR-25.

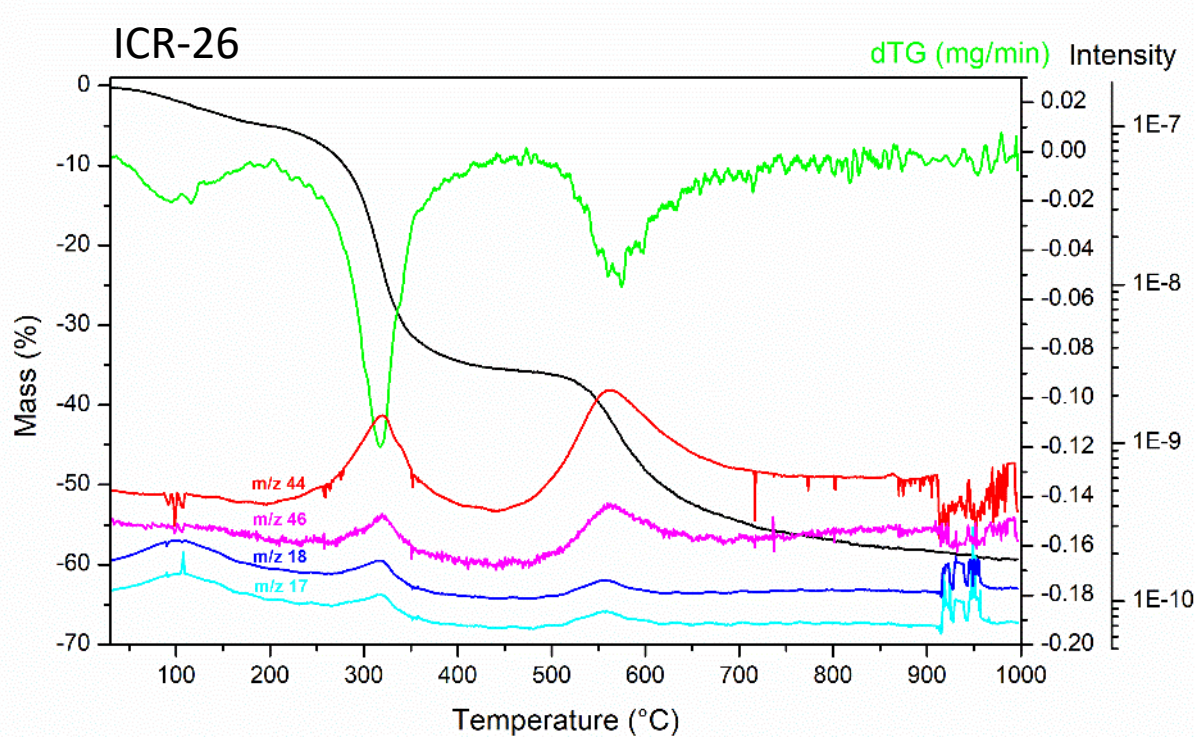

Figure S28: TG/dTG curves and the evolution of gases for ICR-26 on air; m/z = 17 – OH, m/z = 18 – H_2O, m/z = 44 – CO_2, and m/z = 46 – NO_2.

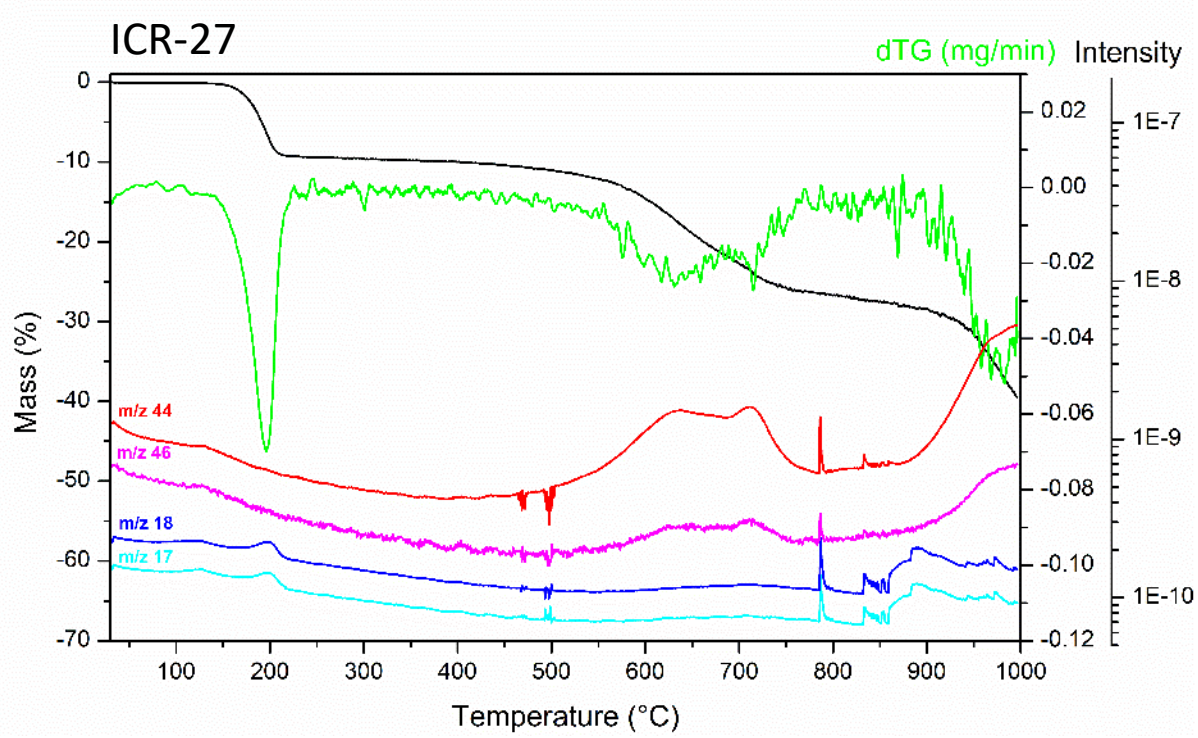

Figure S29: TG/dTG curves and the evolution of gases for ICR-27 on air; m/z = 17 – OH, m/z = 18 – H_2O, m/z = 44 – CO_2, and m/z = 46 – NO_2.

Adsorption measurements

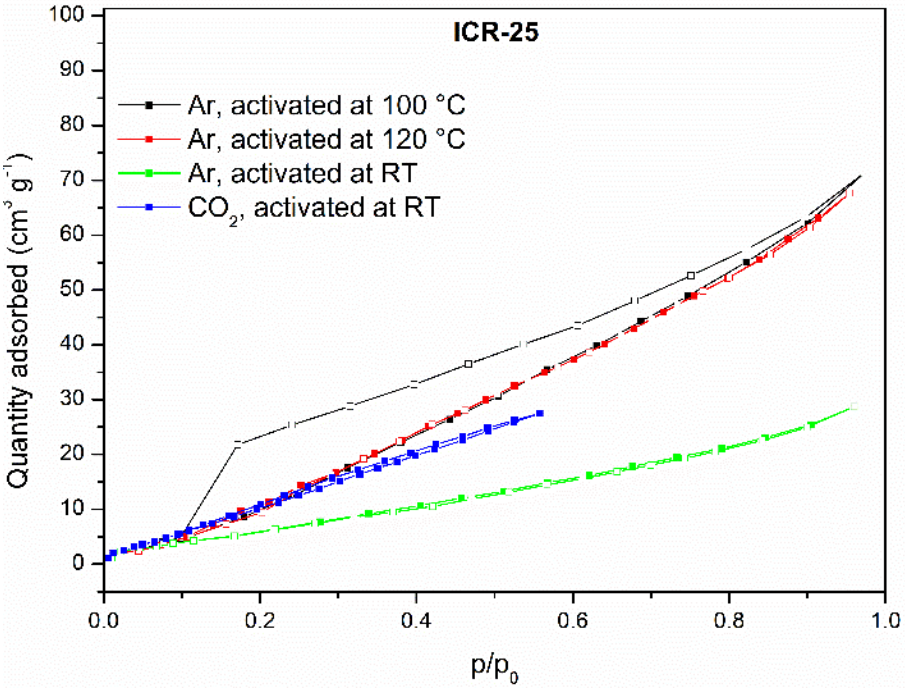

Figure S30: Adsorption isotherms of argon for ICR-25 measured after activation at 100 °C and 120 °C.

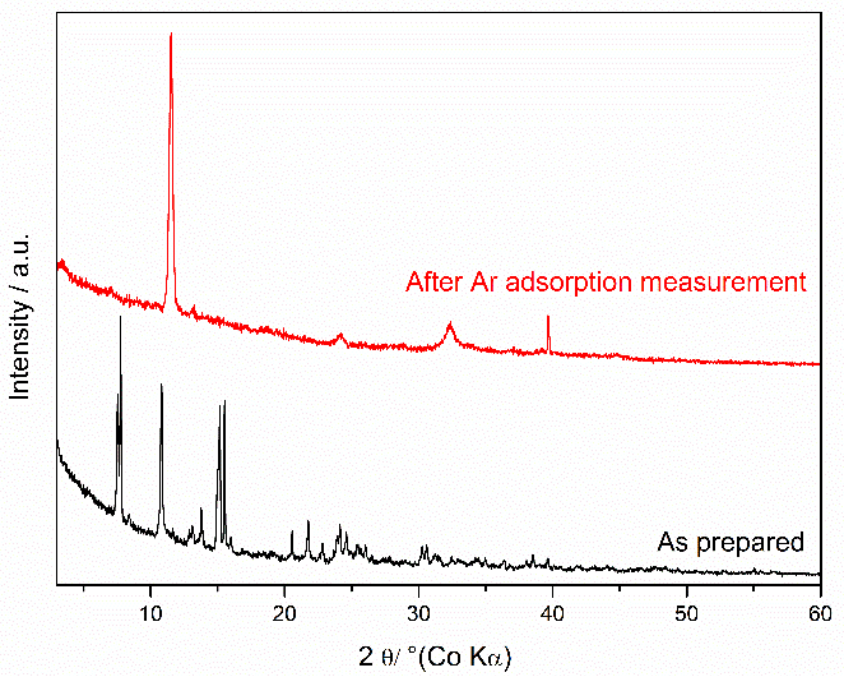

Figure S31: Comparison of the powder XRD pattern if ICR-25 before and after the adsorption measurements.

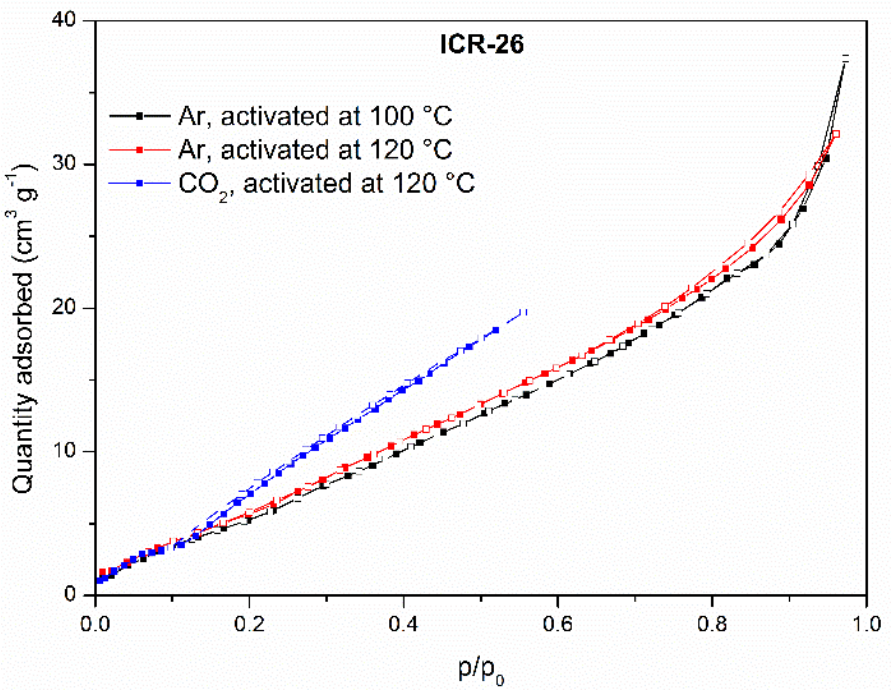

Figure S32: Adsorption isotherms of argon and CO_2 for ICR-26 measured after activation at 100 °C and 120 °C.

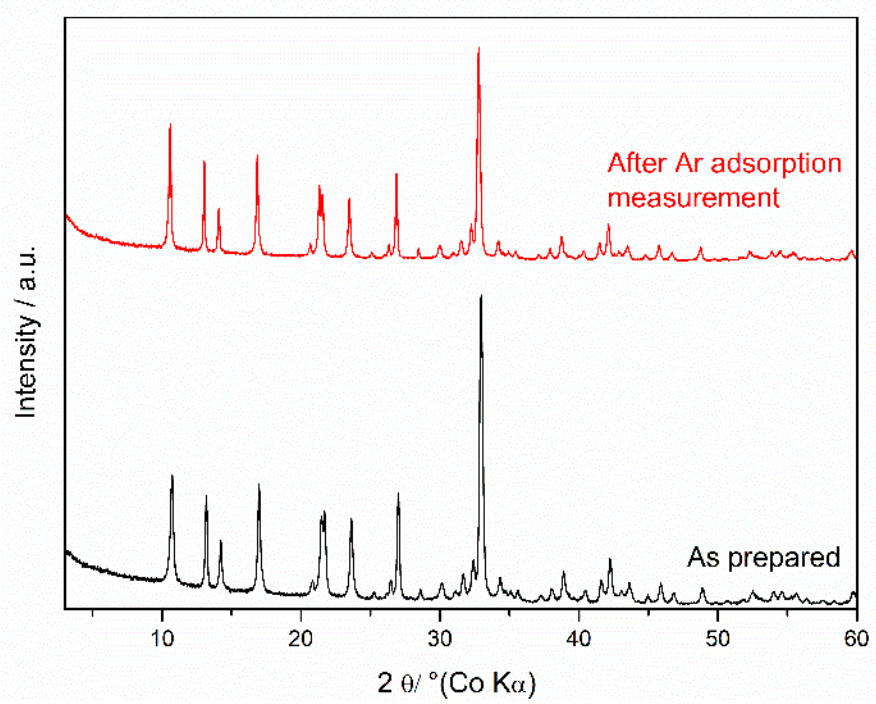

Figure S33: Comparison of the powder XRD pattern if ICR-25 before and after the adsorption measurements.

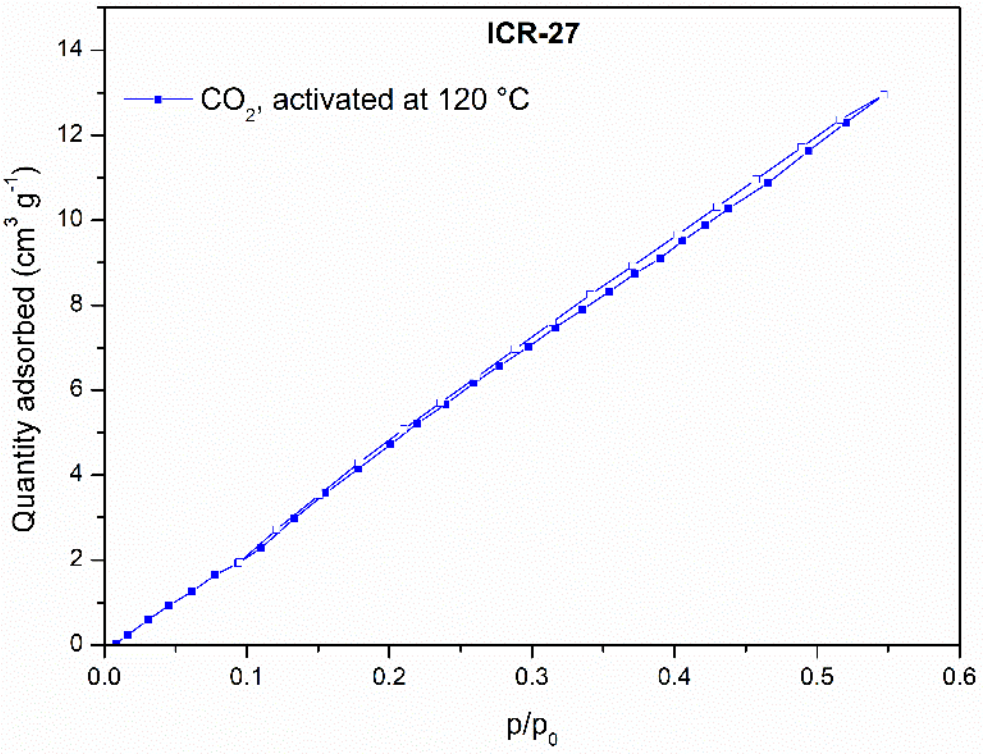

Figure S34: Adsorption isotherms of argon and CO_2 for ICR-27 measured after activation at 100 °C and 120 °C.

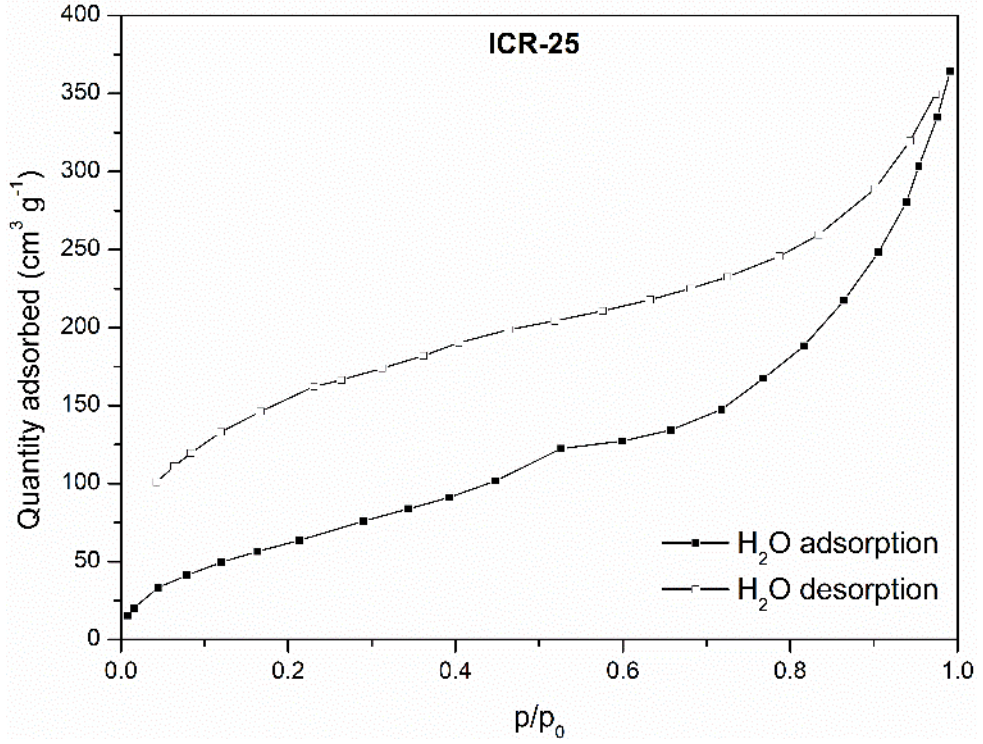

Figure S35: Adsorption isotherm of water for ICR-25 measured after activation at room temperature.

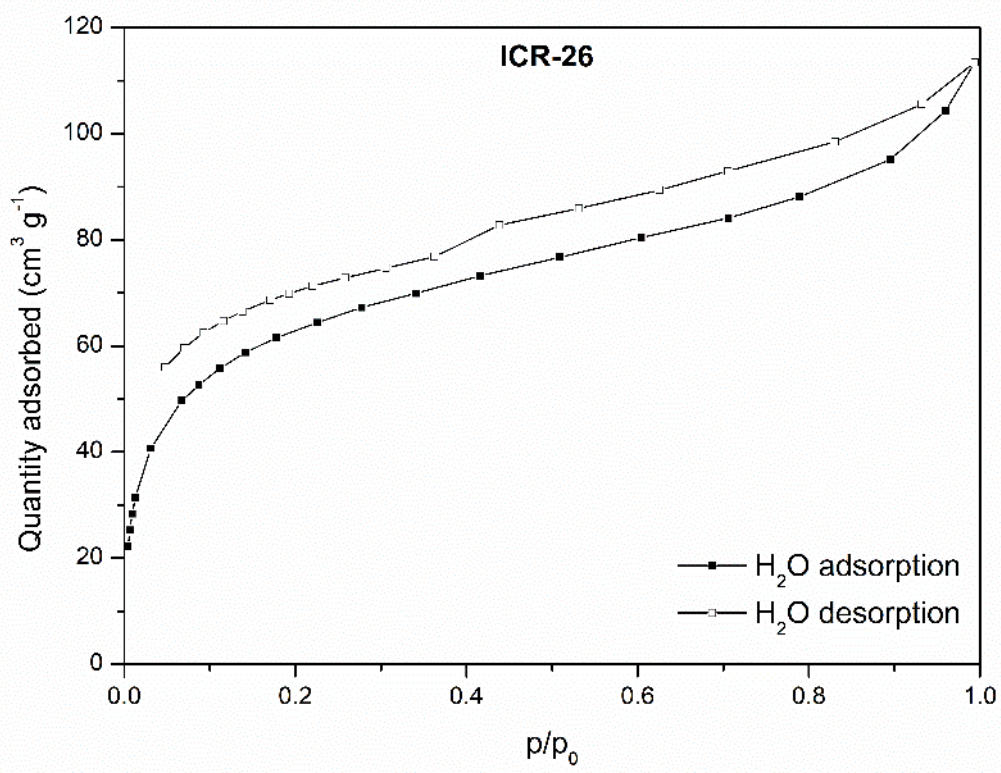

Figure S36: Adsorption isotherm of water for ICR-26 measured after activation at 120 °C.

Phase transition in ICR-25

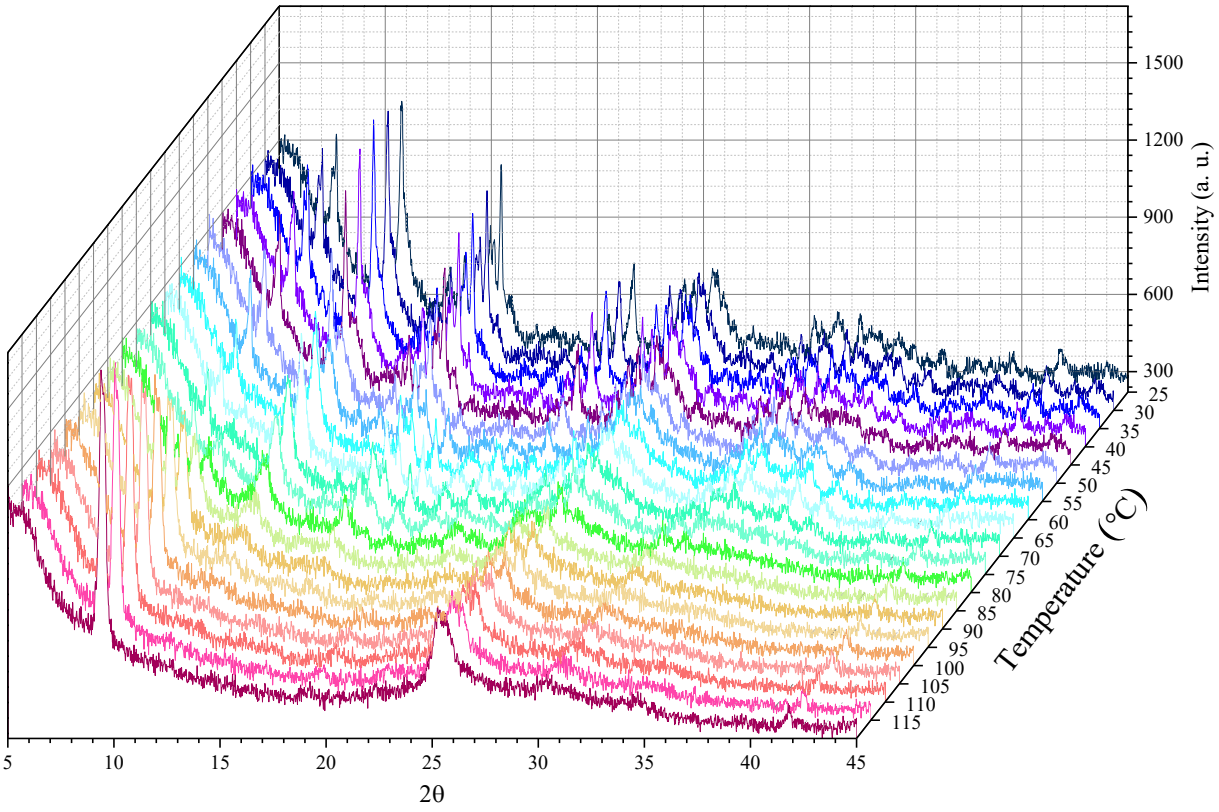

Figure S37: Powder XRD patterns for ICR-25 measured at variable temperature in the range of 25 – 120 °C.

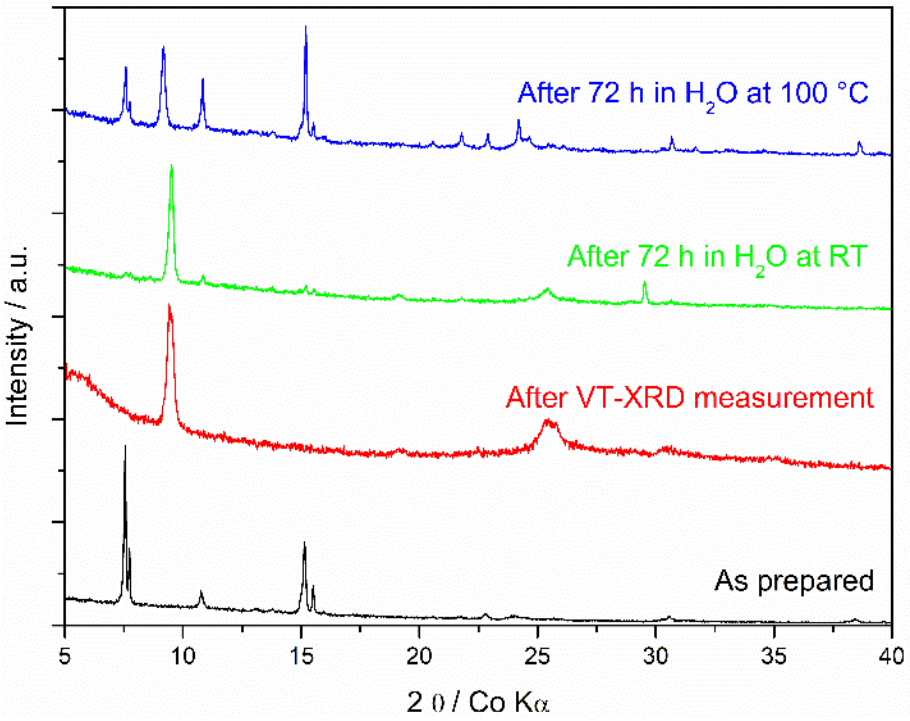

Figure S38: Comparison of powder XRD patterns for ICR-25 measured at the beginning (black), after VT-XRD measurement (red), after 72 h of immersion in water at RT (green), and after 72 h treatment with water in autoclave at 100 °C (blue).

Proton conductivity

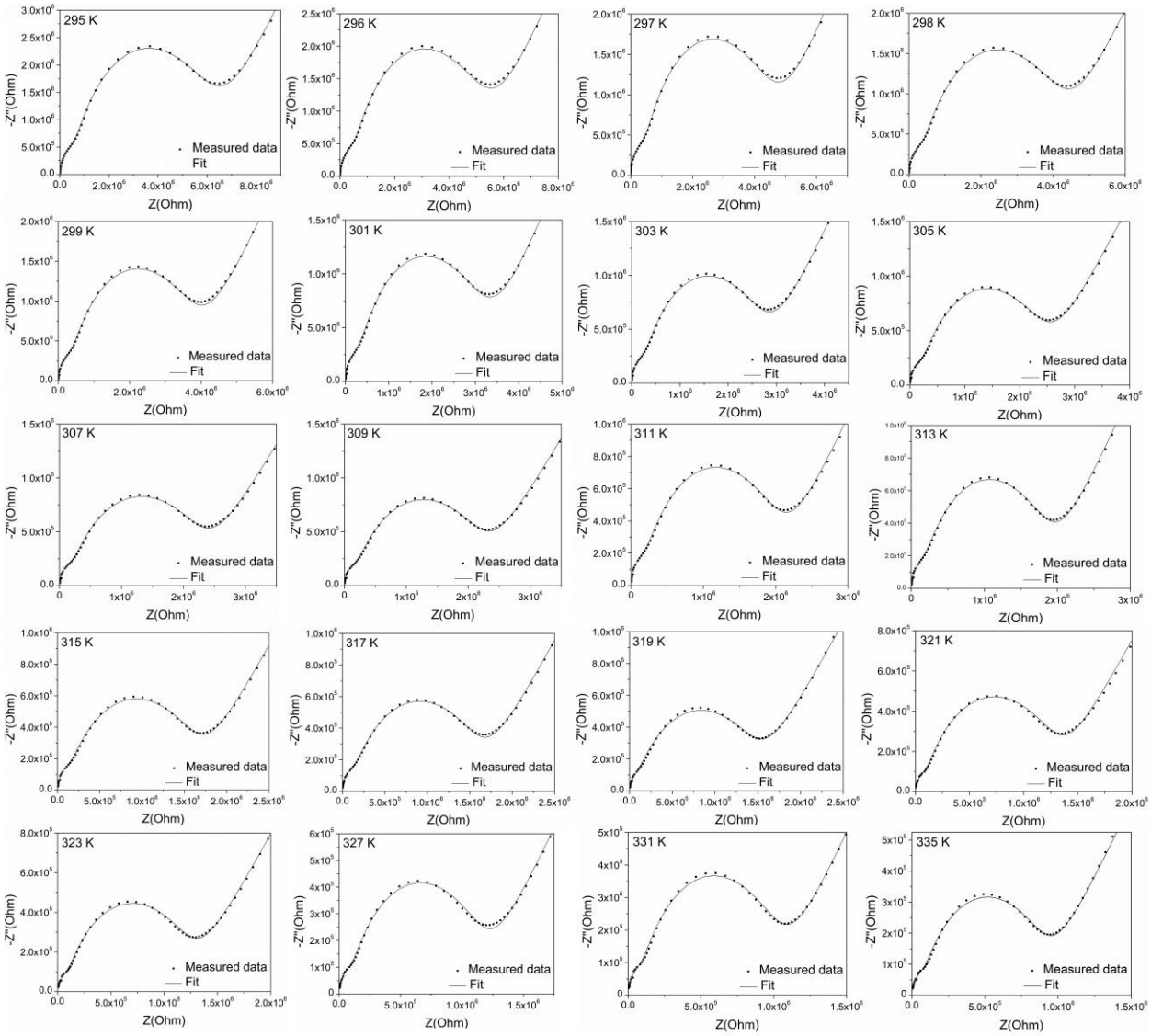

Figure S39: Detailed view of the Nyquist plots for ICR-25 at 75% relative humidity measured at various temperatures and the corresponding fits.

Stability of the materials upon proton conductivity measurement

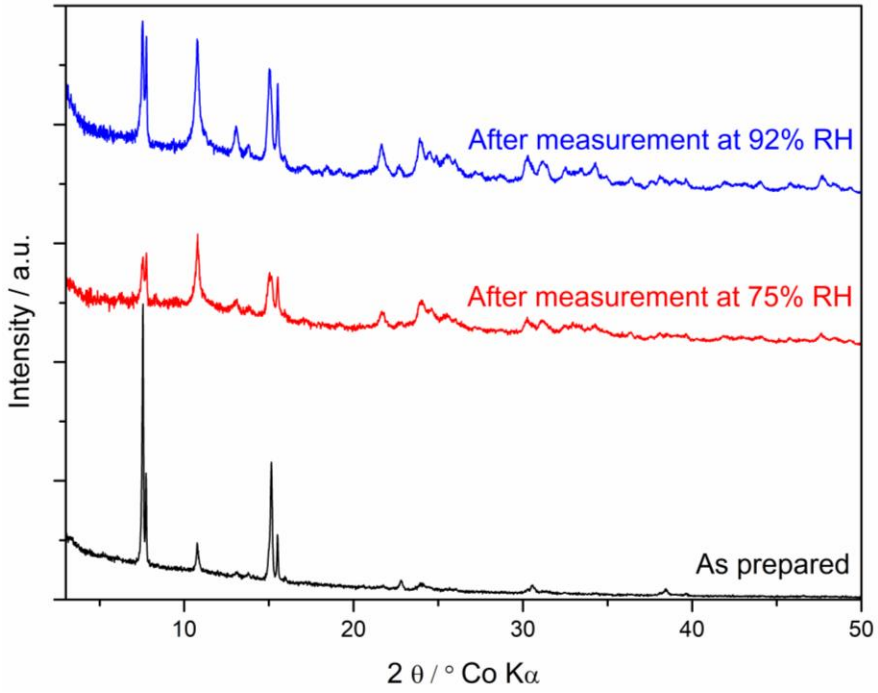

Figure S40: Powder XRD pattern of ICR-25 before (bottom) and after the measurement of proton conductivity at 75% (middle) and 92% (top) relative humidity.

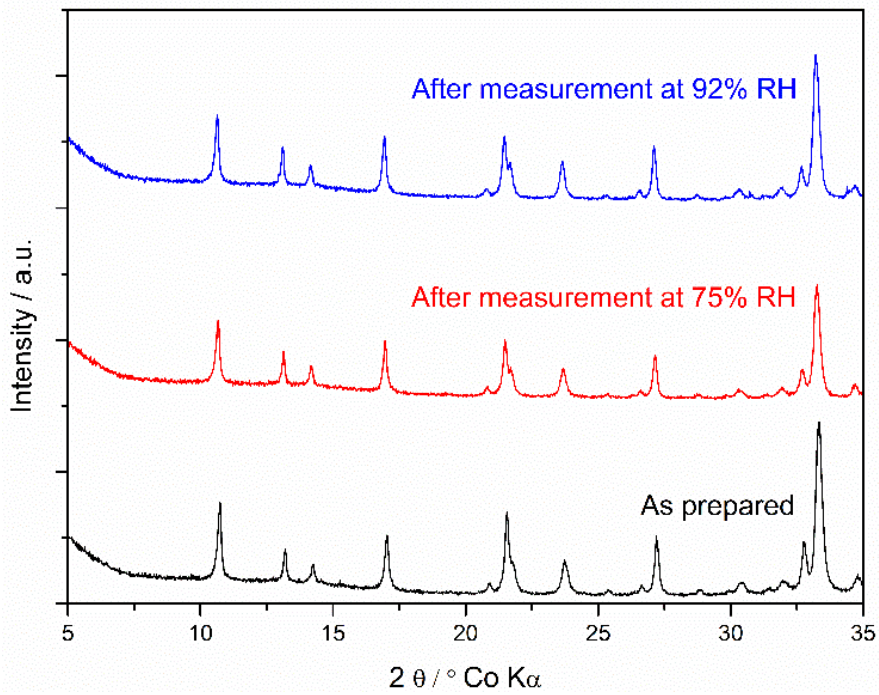

Figure S41: Powder XRD pattern of ICR-26 before (bottom) and after the measurement of proton conductivity at 75% (middle) and 92% (top) relative humidity.

Supplementary tables

Table S1: Crystallographic parameters of ICR-25, ICR-26, and ICR-27.

Compound	**2**	**ICR-25**	**ICR-26**	**ICR-27**
CCDC No.	2503831	2499447	2499450	2499442
Empirical formula	$C_{18}H_{26}N_2O_6P_2$	$C_{40}H_{79}Ca_9N_8O_{75.5}P_{16}$	$C_7H_3AlNO_{8.4611}P$	$C_5H_5MgNO_4P$
Formula weight	428.35	2736.35	294.40	198.38
Crystal system	monoclinic	monoclinic	orthorhombic	monoclinic
Space group	$P2_1/c$	$P2_1/n$	$Pmna$	$C2/m$
***a* / Å**	9.6820(2)	13.6870(16)	6.33764(4)	8.3136(6)
***b* / Å**	25.8378(5)	26.63(5)	7.84629(7)	6.5320(4)
***c* / Å**	8.43670(10)	26.88(3)	19.29804(17)	13.3665(9)
***α* / °**	90	90	90	90
***β* /°**	100.935(2)	89.96(3)	90	109.325(8)
***γ* / °**	90	90	90	90
Volume / Å^3	2072.22(7)	9797(21)	959.633(13)	684.96(9)
Z	4	4	4	4
Density / g cm^{-3}	1.373	1.855	2.0379	1.924
M / mm^{-1}	2.232	7.829	3.95	4.282
F(000)	904.0	5596.0	591	404.0
Crystal size / mm	0.437 × 0.142 × 0.106	0.28 × 0.04 × 0.03	-	0.065 × 0.053 × 0.017
2Θ range for data collection / °	6.842 to 160.018	4.672 to 136.502	-	7.008 to 136.32
Reflections collected	21244	51664	-	1761
Independent reflections	4407 [R_{int} = 0.0562, R_{sigma} = 0.0293]	16655 [R_{int} = 0.2216, R_{sigma} = 0.2092]	-	681 [R_{int} = 0.0212, R_{sigma} = 0.0260]
Data / restraints / parameters	4407/0/268	16655/14/1283	-	681/0/71
Goodness-of-fit on F^2	1.064	1.087	3.8872	1.097
***R* [*I*>=2σ(*I*)]**	R_1 = 0.0532, wR_2 = 0.1502	R_1 = 0.1358, wR_2 = 0.3313	0.0585	R_1 = 0.0346, wR_2 = 0.0986
***R*$_w$ (all data)**	R_1 = 0.0555, wR_2 = 0.1526	R_1 = 0.2430, wR_2 = 0.4053	-	R_1 = 0.0381, wR_2 = 0.1009
Largest diff. peak / hole e Å^{-3}	1.01/-0.65	1.56/-1.24	0.35/-0.50	0.79/-0.41

Table S2: Elemental composition of the prepared coordination polymers determined by CHN combustion analysis. The theoretical composition calculated based on the empirical formula $C_{80}H_{118}Ca_{18}N_{16}O_{125}P_{32}$ for ICR-25, $C_7H_3AlNO_{8.461}P$ for ICR-26, and $C_5H_5MgNO_4P$ for ICR-27 is shown in the brackets.

	C (wt%)	**H (wt%)**	**N (wt%)**
ICR-25	17.88 (17.56)	2.81 (2.91)	4.33 (4.10)
ICR-26	26.46 (28.55)	2.43 (1.02)	4.86 (4.76)
ICR-27	29.06 (30.27)	2.45 (2.54)	7.05 (7.06)

Table S3: Proton conductivity values for ICR-25 and ICR-26 at various temperature and relative humidity of 75% and 92%.

Temperature / K	**ICR-25**		**ICR-26**	
	RH 75%	**RH 92%**	**RH 75%**	**RH 92%**
295	7.0E-07	-	-	1.4E-04
296	8.0E-07	-	6.7E-06	1.4E-04
297	9.1E-07	2.0E-06	7.5E-06	1.5E-04
298	9.9E-07	2.2E-06	-	-
299	1.1E-06	-	8.4E-06	-
300	-	2.8E-06	-	1.8E-04
301	1.2E-06	-	9.2E-06	-
302	-	3.0E-06	-	-
303	1.4E-06	3.3E-06	9.4E-06	2.0E-04
305	1.6E-06	**3.4E-06**	9.9E-06	-
306	-	-	-	**2.0E-04**
307	1.6E-06	3.4E-06	1.0E-05	-
309	1.7E-06	3.3E-06	9.7E-06	1.8E-04
311	1.8E-06	2.9E-06	9.5E-06	-
312	-	-	-	1.4E-04
313	2.0E-06	2.7E-06	9.7E-06	-
315	2.2E-06	2.1E-06	-	-

317	2.5E-06	1.9E-06	**1.1E-05**	9.2E-05
318	-	-	9.8E-06	-
319	3.0E-06	2.0E-06	-	-
321	3.5E-06	-	-	-
322	-	-	-	5.8E-05
323	3.7E-06	2.1E-06	9.2E-06	-
327	**3.9E-06**	2.2E-06	-	7.6E-05
328	-	-	9.0E-06	-
331	4.1E-06	3.0E-06	-	-
333	-	-	9.1E-06	7.2E-05
335	4.6E-06	3.3E-06	-	-
337	-	-	-	7.6E-05

Literature

[1] R. K. Harris. E. D. Becker, S. M. Cabral de Menezes, R. Goodfellow, P. Granger, NMR nomenclature. Nuclear spin properties and conventions for chemical shifts (IUPAC Recommendations 2001) ,*Pure Appl. Chem* 2001, **73**, 1795–1818.